2016

An investigation into the effects of underwater bubble formations on sound speed and attenuation

King, E.

The Plymouth Student Scientist

University of Plymouth

An investigation into the effects of underwater bubble formations on sound speed and attenuation

Erin King

Project Advisor: Sarah Bass, School of Marine Science and Engineering, University of Plymouth, Drake Circus, Plymouth, PL4 8AA

Abstract

Underwater bubbles are prevalent in the marine environment, from natural sources such as breaking waves, biological and geological activity, and artificial sources such as wash from vessel motion and cavitation. Bubbles can remain entrained within the water column for long periods. Due to the attenuative properties of bubbles and the changes to the sound speed profile their presence causes, bubble clouds present a major challenge to commercial sonar operations. These same properties are used positively through implementation of bubble screens to protect structures and wildlife from marine construction operations. This study sought to examine the effects of bubble clouds at different void fractions, and bubble screens at a range of screen separations, upon sound phase speed and attenuation at typical commercial frequencies. 195 kHz and 500 kHz frequencies were tested, and the results of both frequencies compared against each other and theoretical expectations. For bubble screens, significant peak phase speed losses were found at 195 kHz for screen separations of 3cm. A significant peak attenuation was found at 3cm separation for 500 kHz, however no significant peak was found at 195 kHz. Further investigation into the significance of wavelength upon phase speed through screens was found to be justified. Greater attenuation through bubble clouds at 195 kHz matched theoretical expectations relating to bubble resonance. Phase speed results were also found to match theoretical predictions and results gathered from natural bubble plumes. The range of frequencies tested was limited, and frequency recommendations were made for future testing.

Equations

1. Minnaert resonance equation:

$$f_0 = \frac{1}{2\pi a}\sqrt{\frac{3\gamma P_A}{\rho}}$$

2. Sound speed as a function of Frequency and Wavelength:

$$c = f\lambda$$

3. Sound speed as a function of distance and time:

$$c = \frac{d}{t}$$

4. 95% confidence limits for predicted y values interpolated from a linear trend subject to random variations in the contributing data:

$$\left(\hat{m}x_p + \hat{b}\right) \pm t_{a/2,n-2}s_{y,x}\sqrt{1 + \frac{1}{n} + \frac{\left(x_p - \bar{x}\right)^2}{SS_{xx}}}$$

5. Void fraction of the water column for a series of bubble screens:

$$\alpha_w = \frac{Air\ Volume}{Total\ Volume} = \frac{nb \times \frac{4}{3}\pi r^3}{d \times 0.1^2}$$

6. Sound speed within the boundary of a system of bubble screens:

$$V_{cloud} = \frac{0.8}{0.01ns}\left(V_{measured} - V_{reference}\right) - V_{reference}$$

7. Bubble cloud void fraction:

$$Void\ Fraction, \alpha = \frac{nb \times \frac{4}{3}\pi r^3}{0.01n \times 0.1^2}$$

8. Equation 7 for bubble radius, r = 0.0015m:

$$\alpha = 4.5 \times 10^{-5} \pi b$$

9. Attenuation decibel level as a function of relative intensity:

$$\alpha = -20 \log_{10} \left(V_n / V_0 \right)$$

10. Transmission Loss determination from active SONAR equation:

$$TL = \frac{1}{2} (SL + TS - EL)$$

1.   Introduction

Bubbles are prevalent in shallow waters due to natural causes such as frequent wave breaking, rip currents and biological activity in the near shore, and artificial causes such as vessel movement and cavitation. Bubbles can remain in the water column for extended periods due to friction caused by underwater currents and turbulence overcoming buoyancy, coupled with solid and dissolved matter on the bubble surface preventing diffusion of the gas. Bubbles entrained within the water column by these methods tend to be small as larger bubbles rise faster due to a greater buoyant force. Small bubbles have the greatest interaction with sound waves at high frequencies on the order of kHz, in the same range as those used for commercial sonar applications; this interaction comes in the form of attenuation and sound speed change through the water column. These effects have both negative and positive implications for subsea operations.

A major negative effect is interference to commercial sonar operations. Many commercial sonar systems operate at kilohertz frequencies, and are affected by small bubbles resonant at the same frequency. If an active frequency is imposed on a system containing bubbles resonant at that frequency, the bubble oscillates at maximum amplitude, resulting in maximum attenuation from omnidirectional scattering of energy and conversion to heat (Urick, 1967). Sound speed changes can also occur through a water column containing entrained bubbles. Sebastian (2001) examines these effects in the context of multibeam bathymetric sonar operations in the low to high kHz range. Attenuation results in a reduced signal to noise ratio, and a consequent loss of target discrimination; changes in sound speed can reduce the accuracy of calculated ranges. Acoustic interference from bubble clouds has implications for underwater sonar where bubbles created by survey vessel movement, forced underneath the vessel, interfere with the transducer. Transducer facings on modern survey vessels lie within the range of bubble entrainment at less than 10 metres and frequencies of 50 to 95 kHz are most affected, and bubbles resonant at 150 kHz were found at 5 metres depth in some cases. In conditions where bubbles interfere with acoustic survey operations, survey vessels may have to

cease operations incurring extra costs to the company and/or client. Developing a greater understanding of bubble cloud interactions with sound at commercial frequencies may facilitate future developments to mitigate these negative effects.

Bubbles also have positive applications. Bubble screens have been implemented in a manner to reduce the echo of submarines since methods were pioneered by the Germans in the Second World War as a means of allowing U-boats to escape (Giese, 1994). Bubble screens also have applications in subsea construction, using their attenuative properties for preventing damage to submerged structures from industrial explosives and reducing the impact of operations such as drilling and percussive piling on sound sensitive marine life (Domenico, 1982; Würsig, 1999). A greater understanding of bubble acoustics in the context of artificial bubble formations such as screens will aid in developing future technologies to combat the complications experienced today. This study will examine the effects of two kinds of bubble formation on sound speed and attenuation: single bubble thickness screens and bubble clouds.

2. Aims and objectives

2.1. Aims

1. To examine the effect of bubble screens and clouds upon the speed of sound underwater.

2. To examine the effect of bubble screens and clouds upon sound attenuation underwater.

2.2. Objectives

A. To measure the sound speed at different frequencies in the presence progressively increasing numbers of bubble screens at a range of separations.

B. To measure the sound speed at different frequencies in the presence of a uniform bubble cloud at a range of void fractions.

C. To measure attenuation at different frequencies in the presence progressively increasing numbers of bubble screens at a range of separations.

D. To measure attenuation at different frequencies in the presence of a uniform bubble cloud at a range of void fractions.

The following report outlines the current background research relevant to these aims, the methodology implemented to achieve them and the results, analysis and conclusions drawn in their context.

3. Literature review

3.1. Acoustic theory

Acoustic waves are longitudinal pressure waves. The wave constitutes a density variation in an elastic medium and speed of propagation is governed by the compressibility of the medium through which the wave travels (Leighton, 2004; Lurton, 2002); A more compressible medium will transmit sound slower than a less compressible one. Compressibility is dependent upon the density and bulk modulus of a medium. For water, density is affected by temperature, salinity and pressure, thus these are the governing properties affecting the compressibility, and hence the sound speed, in the absence of other interfering factors such as bubbles. The baseline sound speed measured during this experiment will be governed by these factors, therefore it is important to appreciate the magnitude of the effect variations in each parameter may cause.

Several theoretical models have been established predicting the effects of temperature, salinity and pressure on sound speed (Coppens, 1981; Mackenzie, 1981; Chen and Millero, 1977; Del Grosso, 1974). Each of these approximations has a limited range of applicability. From these, it is possible to determine that in the parameters of this experiment, a temperature increase of 1℃ will result in a sound speed increase of ~4ms^{-1}. The depth and salinity remain constant in this experiment, however temperature variations may be experienced on the order of 1-2℃ over the course of a day.

The models above apply in the absence of additional interference in the water column. The presence of bubbles in the water column has a further effect upon sound speed and attenuation. For frequencies higher than the resonant frequency of the bubbles, a peak relative change in sound speed is reached, before converging logarithmically towards zero. It has been shown that at very high frequencies, where the frequency of sound is large relative to the bubble resonant frequency, the speed of sound not affected by the presence of bubbles in the water column (Medwin, 1998; Leighton, 1994). The same is seen for frequencies much lower than the resonant frequency. Below the resonant frequency, a minimum sound speed is reached before the speed converges towards an asymptote speed below the reference bubble-free speed. This is illustrated in figure 3.1:
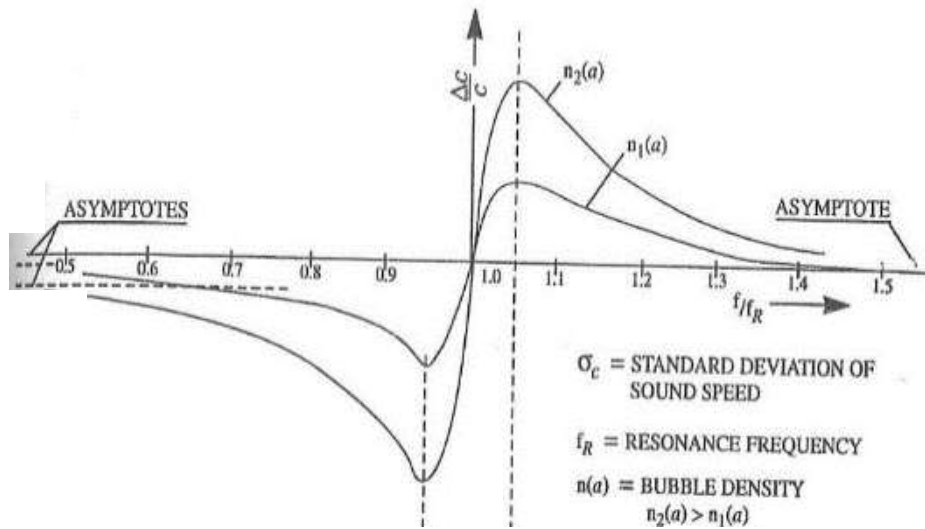
Figure 3.1: Graph depicting sound speed as a function of frequency relative to the resonant frequency of a specific size of bubble in clouds of two different void fractions (Medwin et al, 1975). Reproduced with permission from the American Geophysical Union.

The speed of sound in a medium is dependent upon the compressibility of the medium. For a medium of water with entrained air bubbles, the compressibility of the combined air-water mixture is greater than that of bubble free water. It therefore follows that the sound speed will be less in the presence of bubbles.

In reality, as the compressibility of air is in orders of magnitude greater than the compressibility of water, a small fraction of air in the system results in a considerable drop in sound speed. With sufficiently small bubbles suspended in the water, the liquid may be modelled as homogeneous with a density equal to the proportional average of the air-water mixture. Assuming no resonance effects, the theoretical velocity can be calculated for different void fractions (proportions of air to water) and plotted as a curve. A 1% fraction of air gives a rough drop in theoretical sound speed from 1500 ms^{-1} to 100ms^{-1} (Wood. 1930). Therefore the sound speed changes expected when investigating the second aim of this experiment are likely to be large at high void fractions, however the assumption of homogeneity may not be applicable to relatively large radius bubbles.

Wood's model assumes no resonance, however resonance is an important factor in the effect of bubbles on sound speed. A bubble at resonance will attenuate sound greatest. A bubble of diameter a has a natural resonant frequency known as the Minnaert frequency (Minnaert, 1933):

$$f_0 = \frac{1}{2\pi a}\sqrt{\frac{3\gamma P_A}{\rho}} \tag{1}$$

Where f_0 = resonant frequency, a = radius of bubble, γ = polytropic coefficient, P_A = ambient pressure and ρ = fluid density.

This results in bubble resonances as depicted in figure 3.2 (Weber, 2006). Large bubbles of radius greater than 0.5mm have low resonant frequencies relative to commercial high frequency sonar operating frequencies. This suggests that bubble

resonance is unlikely to play a significant part in sound speed and attenuation change in this experiment.
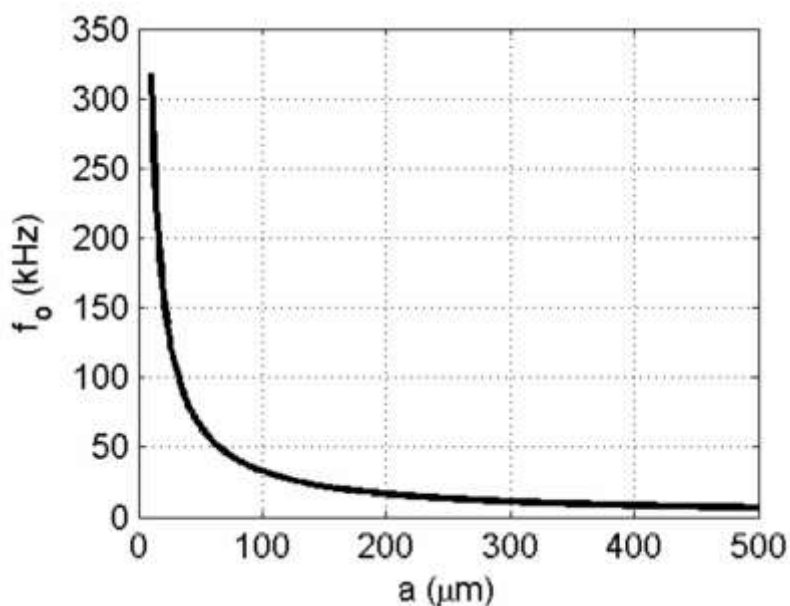

Figure 3.2: Bubble resonant frequency as a function of bubble radius. Reproduced with permission from (Weber, 2006).

To further establish if resonance will play a significant part in this experiment, it is necessary to examine the effects of resonance and the proximity of the applied frequency to a bubbles resonant frequency on sound speed. For a homogeneous bubble-water mixture comprised of bubbles of uniform diameter there is a loss in sound speed at frequencies lower than the resonant frequency. At frequencies greater than resonance there is a peak speed, before an asymptotic decay towards the bubble free velocity at high frequencies (Urick, 1967). This demonstrates that sound speed is affected by the frequency of the incident sound wave and the bubble size. It is expected therefore that there will be a greater effect on sound speed at 195 kHz than at 500 kHz in this study.

This experiment will investigate clouds and screens, as opposed to individual bubbles. The resonant frequency of a bubble cloud is lower than that of the individual bubbles due to the clouds larger radius (Hwang, 2000). It can be modelled as a spherical oscillator of equal radius to the cloud with density and compressibility equal to the average of the two media (air and water). Models such as this assume uniformity of the bubble distribution and size within the cloud. Therefore a spherical oscillating bubble cloud may not be an ideal or realistic model for many applications, including this experiment.

To model bubble screens, a theoretical study by Lu (1990) covers several simple geometries of bubble cloud including a 2 dimensional layer of bubbles. Considering a sound wave propagating perpendicular to the plane of the bubble layer, the situation is reduced to a single dimensional problem. Two situations were considered: a plane of bubbles in an infinite liquid mimicking a plane of bubbles entrained through Langmuir circulation, and a plane of bubbles layered just beneath the surface. In the context of the experiment to be carried out, the first scenario is most relevant. The theoretical phase speed of sound in a 1% mixture of air to water as a function of

frequency for bubbles of varying radius is such that at the Minnaert frequency of the bubble there is a corresponding phase speed minimum through the mixture.

Complex equations are solved by Lu (1990) to give a theoretical natural frequency for a bubble layer (calculated from the real term of the Eigen frequencies) as a function of void fraction. The results of these calculations show a collective resonant frequency significantly lower than the frequency of the individual bubbles. A comparison is also made between bubbles of radius 1 mm and 0.1 mm for two Eigen frequencies showing that in the third mode the Eigen frequency of the layer corresponds closely to the resonant frequency of the 1mm bubble, and the difference between the 1 mm and 0.1 mm bubble results matches with the drop in sound speed seen at the resonant frequency for the 1mm bubble in theoretical phase speed calculations mentioned previously.

An analysis of how the clouds resonant frequency changes with respect to the thickness of the bubble layer was made by Lu. Bubble layer thickness has a substantial effect, lowering the resonant frequency of the layer. This may have implications later with regards to this experiment; as bubble layers get closer together they may be begin to act as a single thicker layer.

Another benefit of using this model is the bubble sizes in this model correspond more closely to the bubble sizes likely to be encountered in the experiment than models which assume small bubbles and a homogeneous fluid. These models do assume homogeneous bubble distributions, which is unrealistic in the majority of instances. This has implications as the propagation of sound in a system containing a randomly scattered bubble cloud, or a series of bubble screens, will not have an isotropic sound propagation characteristic through it (Nikolovska, 2007). A series of bubbles close together may form a chain. In the case of a bubble chain, bubbles may act in the same manner as a series of masses in a Newton's Cradle, passing the energy from one end of the chain to the other with a lesser reduction in amplitude as would be seen from spherical propagation; sound is transmitted anisotropically (Manasseh, 2004; Doinikov, 2005). This has implications for the attenuation element of this experiment. Bubble chains also exhibit a reduced sound propagation speed as bubble size becomes larger, and as separations become smaller.

To understand the applications of these models, and the results of this study, to the real world it is important to consider the formations, distributions and effects of bubbles in the natural environment. The following section examines the current literature on natural bubble formations in the context of this study.

3.2. Natural bubble formations

It is important to understand natural bubble formations in order to bring this study into context with the real world. Bubble clouds form as individual bubbles produced by breaking waves are entrained by turbulence and Langmuir circulations (Thorpe, 1982; Farmer, 1994). Bubble layers are injected down through the water column by breaking waves in the surf zone; their effects are seen to be greatest upon higher frequency sounds, as smaller bubbles with a higher resonance remain entrained longest (Farmer, 2001). Frequencies of 12 kHz and 100 kHz were examined using stationary imaging sonar systems. Bubbles injected into the water column by breaking waves were found to be the primary cause of signal loss in the surf zone,

and the time the bubbles remained entrained in the water column was longer than the time between successive breakers. Closer to the surface, where more bubbles were present, the effect was greatest upon the high frequency sonar. Lower frequency sonar was less impacted, as the lower resonant frequency corresponds to larger bubbles which rise quicker through the water column. There is a basis for an argument to understand more about the characteristics of bubble layers and formations in this context. It may be expected that the highest frequency in this experiment will be attenuated least, as the bubbles produced are resonant at a much lower frequency.

The effects of bubbles on sonar operations is mostly concentrated near the surface, meaning the most affected systems are those which are hull or pole mounted on survey vessels, or stationary imaging sonar systems in close enough proximity to the surface to be affected. Depth profiles of bubble concentrations in different wind conditions have been investigated, finding bubble concentrations decay roughly exponentially with depth (Crawford & Farmer, 1987). A study by Brekhovskikh investigated a distribution of bubble sizes at different depths showing how smaller bubbles are held deeper in the water column. This is an area for further research, as bubble radii distributions have been little investigated with respect to depth (Brekhovskikh, 2001).

This report investigates the effect on sound speed of artificial bubble formations created in the laboratory. To place this into context within the natural environment it is necessary to consider the effects of natural formations on sound speed. The effect of bubbles in shallow water upon the sound speed at different frequencies is illustrated in an experiment by Lamarre and Melville (1994) (Figure 3.3).

A buoy was fitted with six sound speed measuring modules containing two rigidly mounted omnidirectional hydrophones each (transmitter and receiver), an imaging camera and a temperature sensor. Measurements were taken at 2 Hz over a 20 minute period for frequencies between 6 and 40 kHz with a wind speed of 8 ms^{-1}. One criticism is that the frequency range is small relative to commercial sonar use. At frequencies below 20 kHz, sound speed was frequency independent and the primary factor in reducing sound speed was the change in void fraction due to the bubble plume. At 20 kHz and above it was found that frequency became a significant consideration as bubble resonance effects increased. At 40 kHz the sound speed was seen to increase slightly during bubble plumes, and it was suggested a local peak bubble density could be the cause. This negative anomaly as seen in figure 3.3 emphasises the dominance of bubble resonance in affecting sound speed at the higher frequencies in this experiment (Lamarre & Melville, 1994). A potential way to build on this data set would be to use a wider range of frequencies in a wider variety wind speeds, observing any differences in the sound speed effects of the bubble plumes between different wind speeds.
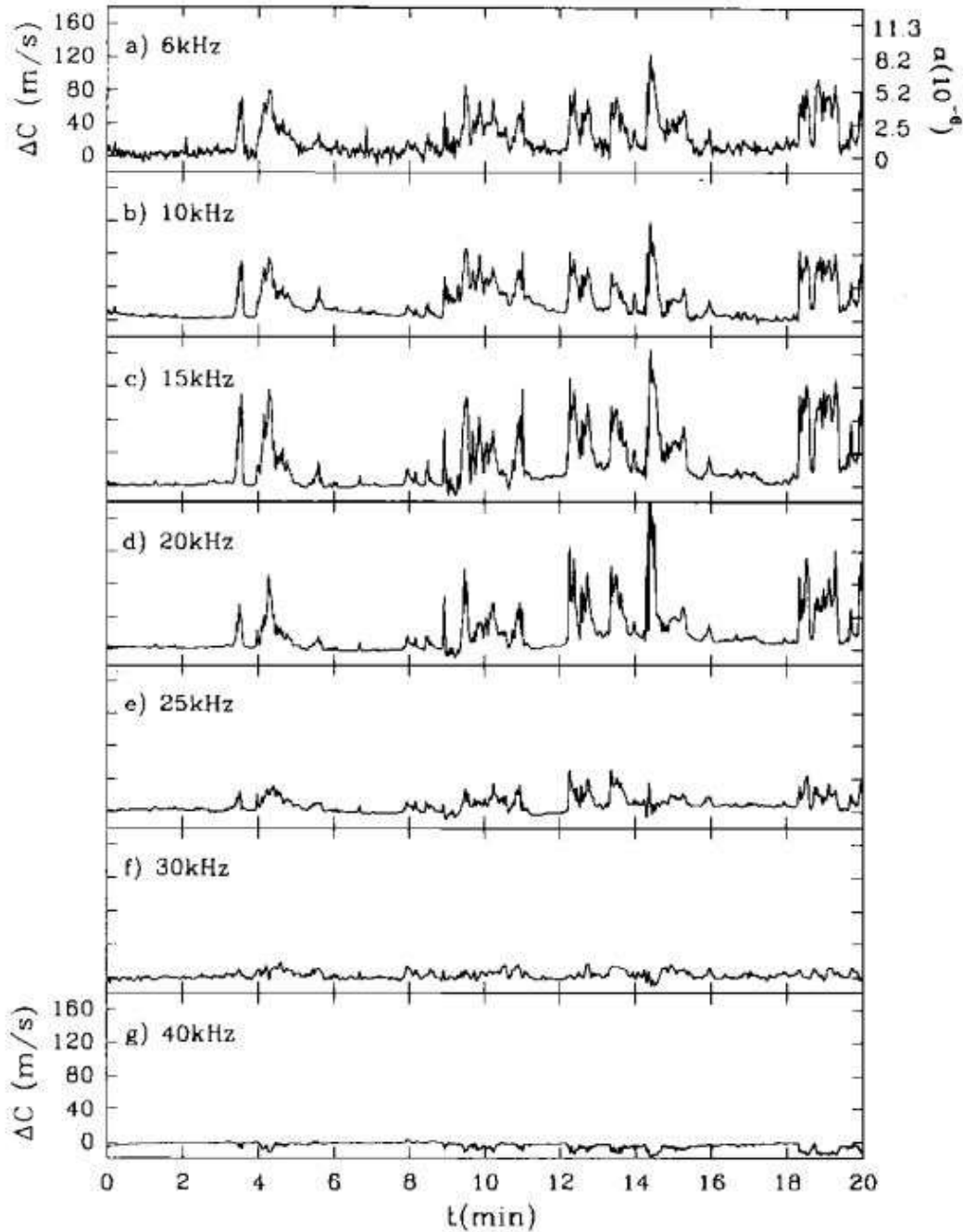
Figure 3.3: The change in sound speed (left axis) over time for the 20 minute period of measurement at frequencies between 6 and 40 kHz taken at a depth of 50 ± 10 cm with a wind speed of 8 ms-1 and the corresponding void fraction (right axis). Reproduced with permission from (Lamarre & Melville, 1994) Copyright (1994), Acoustical Society of America.

Effects on sound speed and attenuation due to bubble screen separation are investigated in this report. In the natural environment, bubble plume spacing has been shown to have an effect upon sound speed and attenuation. Work has been done to model bubble cloud interaction with high frequency sound in the low kHz range with emphasis on oceanic bubble layers under windy conditions, and applications in the higher several hundred kHz range (Boyles, 2013). The effects of natural bubble plumes on sound speed and attenuation are examined in winds of 13.6 ms^{-1} building upon work by Novarini (1998). Bubble plumes have a significant

effect upon sound propagation through the water column, and that plume spacing has an influence upon the sound speed. The plumes are defined as β plumes, with a lifetime of ~4 seconds, evolving from short lived α plumes and decaying into long period γ plumes. α plumes have a negligible effect relative to β plumes. Further work is required to look at the effect of γ plumes on β plume spacing which has a considerable contribution to the overall effect on sound propagation. The size distributions and effects on sound speed and attenuation of these plumes are outlined in a thesis by Weber (2006) (figures 3.4 & 3.5). Bubbles of radius on the order of 1mm are only present in β plumes, and so are relatively short lived in the water column compared to smaller bubbles which make up the γ plumes. Attenuation in β plumes decays sharply between the two frequencies to be investigated in this experiment (195 kHz and 500 kHz) therefore it is expected that attenuation will be greatest at 195 kHz.

In order to develop an effective methodology to model bubble formations in the laboratory, a review of previous laboratory based bubble cloud experiments was conducted. This is outlined in the following section.
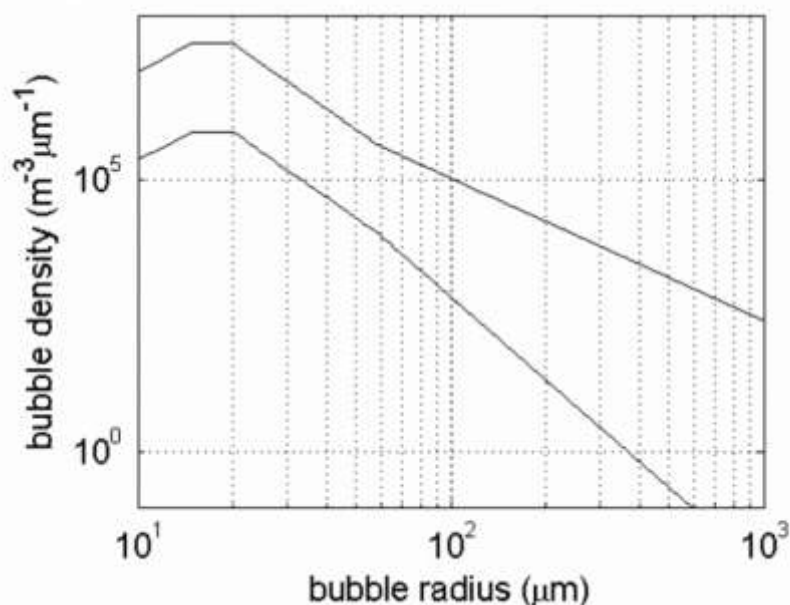

Figure 3.4: Bubble size distribution for β plumes (upper curve) and γ plumes (lower curve) at a wind speed of 15 ms^{-1} at 2 m depth, with void fractions of 8.0 x 10-5 and 1.1 x 10-6 respectively. Reproduced with permission from (Weber, 2006).
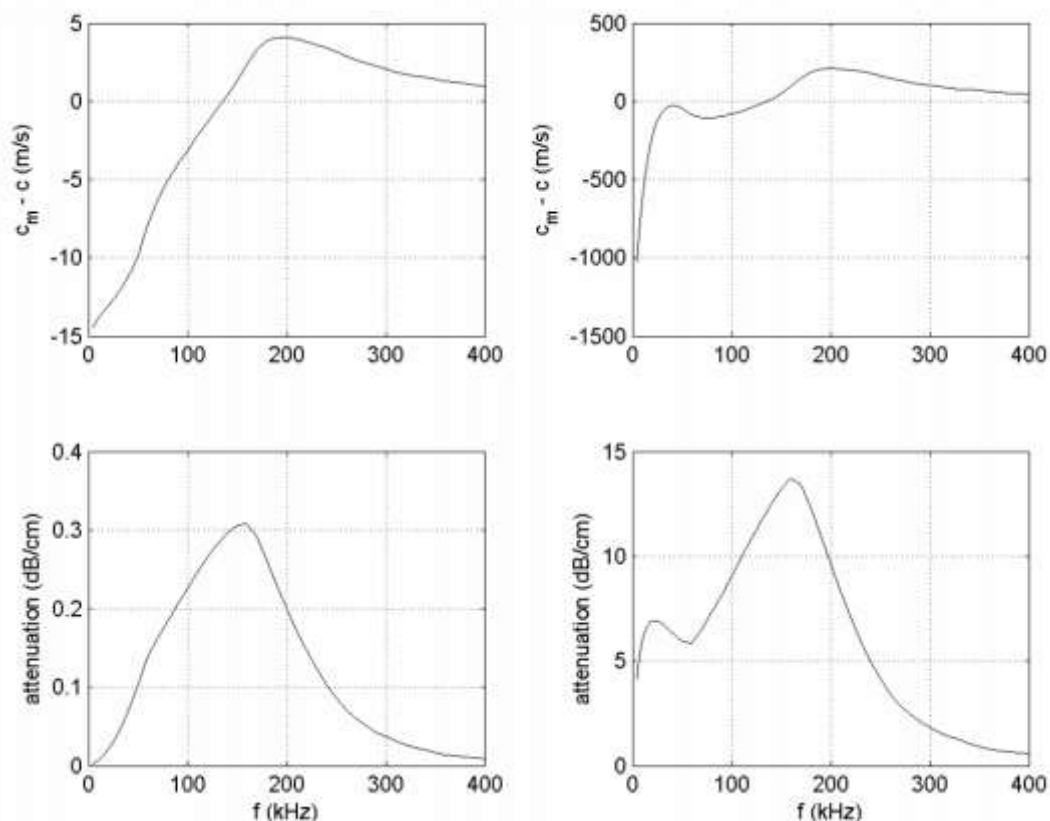
Figure 3.5: Sound speed and attenuation for the γ plumes (left) and β plumes (right) shown in figure 3.4. Reproduced with permission from (Weber, 2006).

3.3. Bubble clouds in the laboratory

Acoustic analysis of bubble clouds has been covered in previous research examining ambient noise characteristics and resonances in a laboratory setting. One study has looked at a cylindrical bubble cloud and produced comparisons with a theoretical model of collective oscillations finding a close agreement with experimental results (Nicholas et al, 1994). Another paper presents an undergraduate level experiment for measuring the sound emitted from a single bubble, and finds the measured frequency to be in accord with the natural resonant Minnaert frequency of the bubble. Comparisons are also made to natural running waters finding the observed acoustic signal to be a series of Minnaert oscillations (Leighton, 1987).

The model presented by Lu in section 3.2 was found to closely match the experimental results of an experiment by Yoon (1991) in which a circular bank of hypodermic needles was placed at the bottom of a water tank, and high pressure air pumped through them creating a cylindrical column of water with variable void fraction by varying the flow rate of the air (Yoon et al, 1991). This method of creating a variable void fraction through a variable air flow presents a less labour intensive way of conducting this sort of experiment than that used in a previous study by Fairman (2014) which involved covering holes in air lines to reduce the number of bubbles output by the line.

A previous thesis conducted by Fairman (2014) examined the effects of bubble screens upon sound speed. This study tested screens at separations from 2.5 cm to

10 cm at a range of bubble densities and found a linear relationship for the rate of sound speed loss as screens are added to the system at separations of 5 cm to 10 cm. At 2.5 cm a non-linear relationship was observed with the rate of speed loss increasing as a function of the number of added screens. It was hypothesised that there may have been the beginnings of exponential growth in the rate of speed loss at this separation (Fairman, 2014). Data collection was limited in scale. Additionally the accuracy of the measurements comes into question, as the measurement device used to measure wavelength used in a speed = distance / time calculation was of the order $\pm$ 1.5 mm resulting in a component error of 15 ms^{-1} in the calculated sound speed, before other contributing errors are taken into consideration. Less error would be carried through the calculations using a speed = frequency X wavelength relationship for the same methodology implemented by Fairman. This will form the basis for phase speed analysis in this experiment.

Sound attenuation and phase speed change around bubble resonance frequencies is covered in a paper by Duro (2011) between 30 and 170 kHz simulating cavitation effects. They vary the frequency of sound transmission through a cloud of micro-bubbles produced by a pressure washer and determine that attenuation and sound speed change are greatest closest to the resonant frequency of the bubbles produced in their experiment (75 kHz) as would be expected in light of the theoretical models described earlier (Duro, 2011).

Under water bubbles are seen to be a significant problem for commercial sonar operations due to the effects of attenuation and changes to sound phase speed. Major causes of bubbles include wave breaking, cavitation at the transducer face, wash from vessel motion, and bubbles caused by the propeller motion. Natural bubble formations have been analysed and modelled; however bubble clouds and screens remain a topic of further study looking at plume formations and interactions. There is scope for further research to examine and model bubble plume acoustics. In the laboratory, theoretical models have been found to match experimental results for collective resonances of bubble formations, though there remains room to expand on the current knowledge in this area. As studying natural bubble formations in the nearshore presents a major experimental undertaking, there is limited data available, and more data acquisition on bubble formation acoustic interactions would help to create a more complete picture. This study will build upon methods described in this section to analyse bubble screens and clouds in order to build on the existing knowledge in this subject.

4. Methods

4.1. **Bubble generation**

It was necessary to devise a method of producing a uniform distribution of bubbles of even size in both stratified bubble screens and a bubble cloud. A method had been devised previously, described in section 3.3, which was used as a basis for refining the procedures used in this experiment (Fairman, 2014). The resulting methodology is outlined below.

4.1.1. Screens

In order to produce bubbles in the water column three components were required: an air source, a diffusion system, and a means of holding the system in place at the bottom of the tank.

An Aquarline Resun Ac-9908 Eight Outlet Air Pump was used as an air source. 6mm aquarium air hosing was used to manufacture the diffusion system. Lines were cut of sufficient length to allow the system to be placed at the bottom of the tank, while remaining suitably short to ensure adequate pressure at the diffuser end. Each line had a no-return valve in the end preventing air escape, while the other end was attached to one of eight outlets on the air pump, allowing for a total of eight air lines. Holes were drilled into each line at 1cm separation, of diameter 0.4mm along a 30cm length, at the end of the line to be laid at the bottom of the tank. These holes allowed air to escape as a screen of bubbles from each line. Smaller than 0.4mm diameter and the pressure of the air pump as insufficient to produce a homogeneous screen, larger and flooding of the line occurred. Lines were attached to the bottom of the tank via a rack comprising a 5mm Perspex sheet marked with a centimetric grid, with brass eyes screwed in at the necessary separations to allow for eight bubble screens at separations from 1cm to 6cm. Suction pads affixed the rack to the glass base of the tank. Figures 4.1 and 4.2 illustrate.
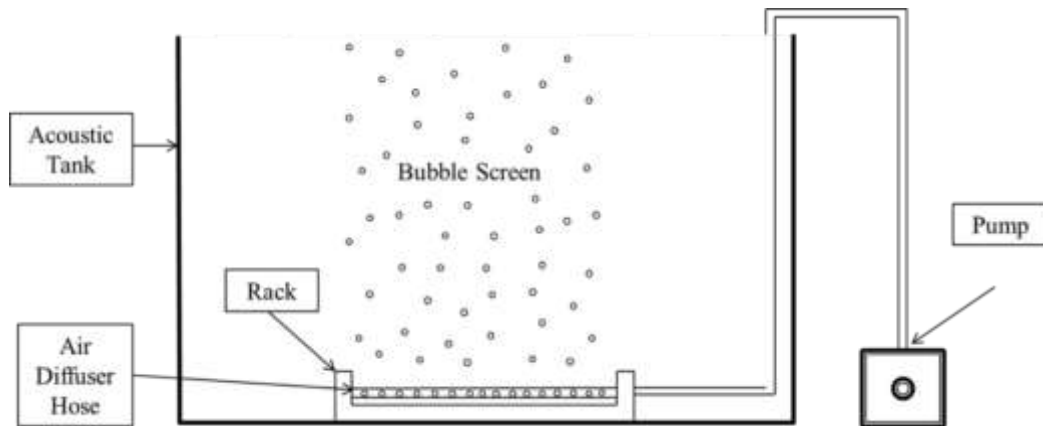

Figure 4.1: Bubble generation schematic, profile view. Reproduced with permission from (Fairman, 2014).

Figure 4.2: Bubble screen generation apparatus. Left: An air pump connects to a single air-line affixed to the bottom of the tank producing a single bubble screen. Right: Eight bubble screens in series at 3 cm separation.

Bubble diffusion results in merging of the bubble screens into a cloud higher in the water column, therefore it was important that any measurements were taken close to the base of the tank to avoid the screens acting a one thick layer as described in section 3.1, or as uniform cloud.

4.1.2. Clouds

As bubbles were produced from holes at 1cm separation along the lines, placing the lines at 1cm separation from each other produced a uniform grid of diffuser holes generating a uniform bubble cloud. A variable air flow was identified in section 3.3 as being the most efficient method for varying cloud void fraction. The variable output of the Aquarline Resun Ac-9908 allowed for variation of the void fraction of the bubble clouds by reducing the air flow. Eight bubble lines were used in the bubble cloud experiments giving a cloud 8cm thick at the output. Bubbles tended to converge higher up in the water column, therefore it was important that measurements were taken close to the output to ensure a uniform bubble distribution.

Measurements were taken of the output from each bubble line at pre-marked output levels. This was achieved by mounting a line at the base of the tank, with a 10x10cm grid behind. High speed images were taken of the bubbles against the grid (figure 4.3) allowing for bubble size and quantity to be determined. This allowed for void fraction to be calculated. Due to the size of the bubbles, and their distributions, homogeneity assumptions described in section 3.1 for theoretical phase speed changes due to void fraction may not be applicable. The size of the bubbles also suggests the attenuation and phase speed effects are most likely to follow those of the β plumes described in section 3.2.
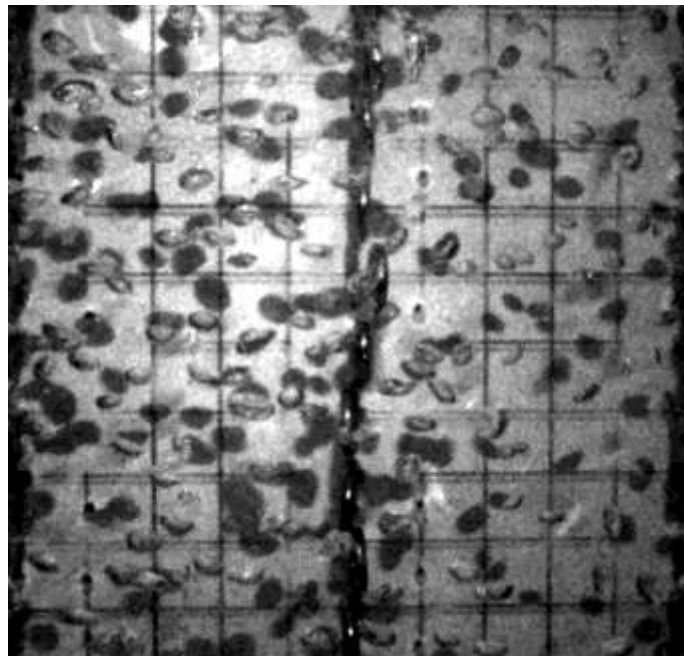

Figure 4.3: Enhanced high speed image of bubbles superimposed against a 10x10cm grid for counting and size estimation.

4.2. Data collection

4.2.1. 195kHz

The Acoustic Systems Trainer (AST) – SONAR was used for measurements at 195kHz of both sound phase speed and attenuation. The AST allowed for viewing of the transmitted and received signals on an oscilloscope trace of Voltage against time. This trace could be averaged to achieve a steady display reading. A transducer was mounted on the wall of the tank, low enough to avoid the effects of bubble diffusion. A hydrophone was placed on moveable trolley in line with the transducer. The setup is shown in figure 4.4.
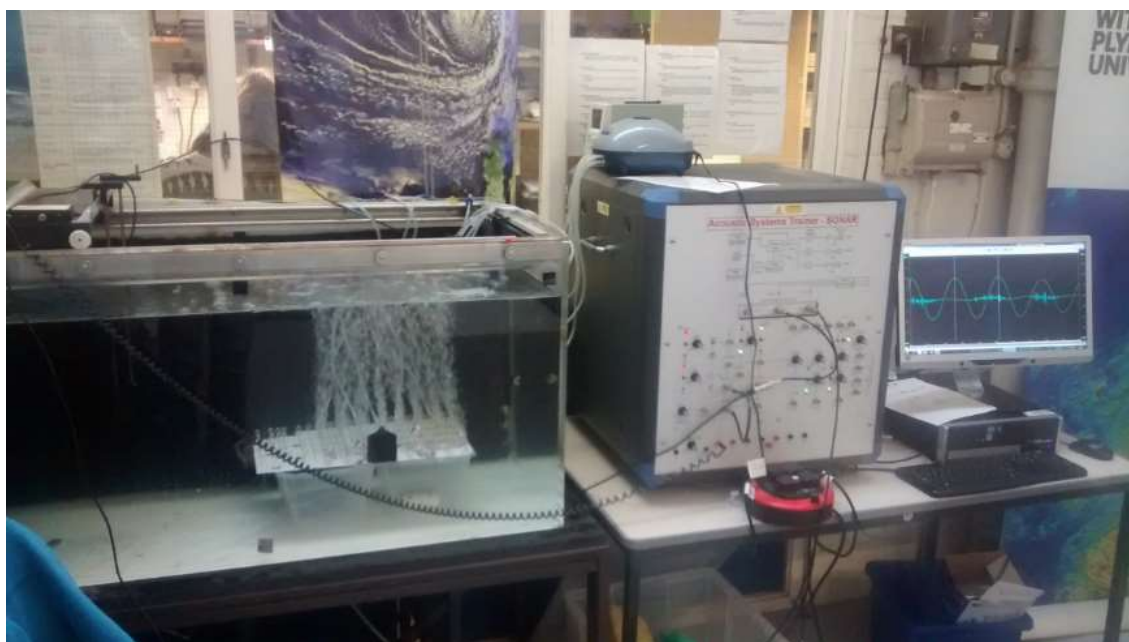
Figure 4.4: Equipment set up for sound speed and attenuation calculation at 195kHz using the Acoustic Systems Trainer – SONAR. Transmitted and received signals are shown on the oscilloscope trace to the right.

4.2.1.1. Sound speed

For reasons of reducing errors described in section 3.3, phase speed measurements were calculated using the formula

$$Speed = Frequency \times Wavelength \qquad (2)$$
$$c = f\lambda$$

Frequency was determined using the time period for 5 oscillations taken from the oscilloscope trace, divided by 5 to give the period for one oscillation, then inversed to calculate the frequency. This gave a frequency of 195 ± 2 kHz.

To calculate wavelength, the pulse width was set to maximum. The hydrophone was moved away from the transducer until the received signal overlapped the transmitted signal on the trace. The trolley was then moved such that the two waves were in phase. This position was marked on the ruler scale alongside the trolley. The

hydrophone was moved away from the transducer a distance of 20 wavelengths, counted on the oscilloscope. This distance was then measured using a set of Vernier callipers accurate to ±0.02mm. This distance for 20 wavelengths was divided to calculate the distance for one wavelength, reducing the impact of any error in measurement. Speed was then calculated from equation 2. This process was repeated three times and averaged to give a final sound speed.

Sound speed was calculated for 1 to 8 bubble screens at integer screen separations of 1cm to 6cm, with a bubble free speed calculated for each series of measurements as a reference ensuring comparability of the data.

The process was repeated for bubble clouds at differing void fractions. 11 outputs were tested giving 11 different bubble cloud void fractions. These fractions were determined as outlined above (Figure 4.3). A reference zero void fraction speed was also taken prior to each experiment.

Speed variations due to temperature fluctuations within the tank during the course of the experiment were recorded using a Valeport mini-SVP Sound Velocity Profiler allowing for quality assurance of the data.

4.2.1.2. Attenuation

A transducer was mounted on the wall of the tank and the hydrophone positioned 0.500m away. The bubble generator was placed between the two. The oscilloscope trace was configured to show the entire transmitted and received pulses, and averaged over 1000 measurements. Using the large cursors tool, voltage readings were taken of the amplitude of the received pulse.

Readings were taken for 1 to 8 bubble screens at integer screen separations of 1cm to 6cm, with a bubble free amplitude recorded for each series of measurements as a reference ensuring comparability of the data.

The process was repeated for bubble clouds at differing void fractions. 11 outputs were tested giving 11 different bubble cloud void fractions. A reference zero void fraction amplitude was also taken prior to each experiment.

4.2.2. 500kHz

At 500kHz data were collected using a Valeport VA500 Altimeter transducer. The transducer was placed on the wall of the tank, and a target positioned 0.500m away in line with the transducer with the bubble formations in between. Data was logged directly and stored through the Valeport Terminal and Datalog X2 software packages (Figure 4.5).

4.2.2.1.   Sound speed

The VA500 Altimeter uses a given sound speed value to calculate a range to the target. This value was set to an arbitrary 1500 ms^{-1}. The range values were then logged for a repeat of 20 readings. These were then averaged. From the equation:

$$Speed = \frac{Distance}{Time} \qquad (3)$$
$$c = \frac{d}{t}$$

The time of travel of the signal was calculated by the distance/1500. This time was then used with the known target range of 0.500m to calculate the speed of sound in the tank. Readings were taken for both screens and clouds as outlined above.
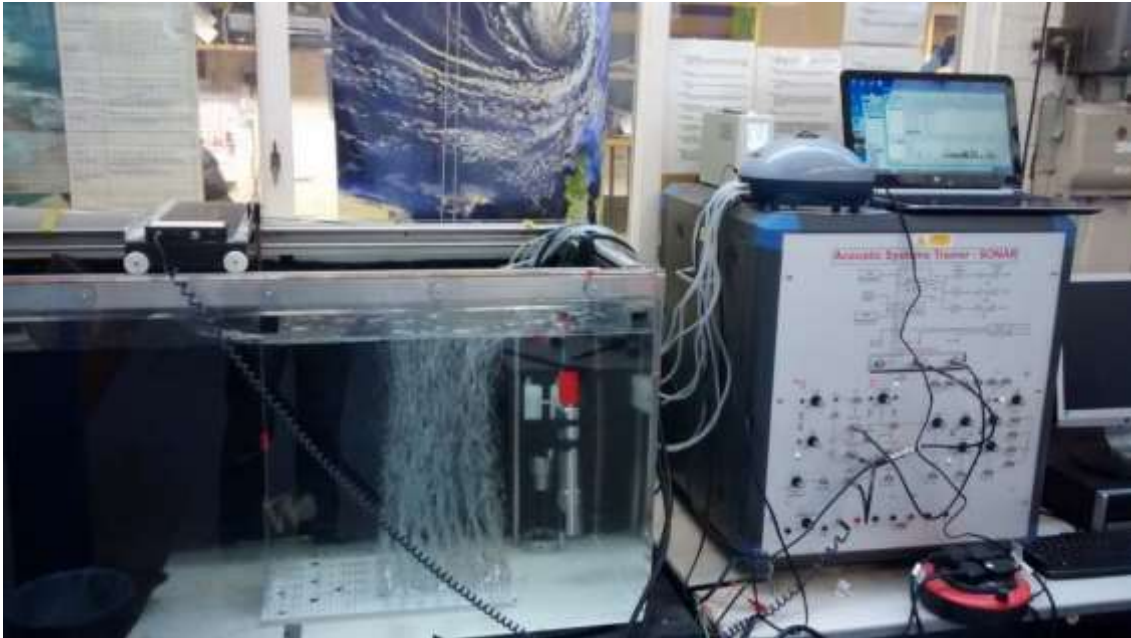

Figure 4.5: Equipment set up for sound speed and attenuation calculation at 500kHz using the Valeport VA500 Altimeter (right of tank). Data was logged automatically to a laptop (top right).

Speed variations due to temperature fluctuations within the tank during the course of the experiment were recorded using a Valeport mini-SVP Sound Velocity Profiler allowing for quality assurance of the data.

4.2.2.2.   Attenuation

A detailed output of all target returns in terms of amplitude and range was possible using the calibration settings of the VA500 Altimeter. This allowed for discrimination between the target and the bubbles to be achieved. Twenty intensity measurements were taken to calculate an average target intensity. Measurements were taken for bubble screens and clouds as above. A visualisation of this un-averaged output is shown in figure 4.6.

Figure 4.6: VA500 amplitude returns and ranges for a bubble free water column (orange) and a water column with 7 bubble screens (blue) at 6cm separation. Returns from individual bubble screens can be distinguished. The target return is considerably lower in amplitude in the presence of bubbles, with some returns lower in amplitude than the returns off the initial bubble layers.

5. Results and discussion

5.1. Phase speed

5.1.1. Screens

Phase speed measurements for each screen separation experiment were averaged and plotted as a function of the number of bubble screens in the system (figure 5.1).
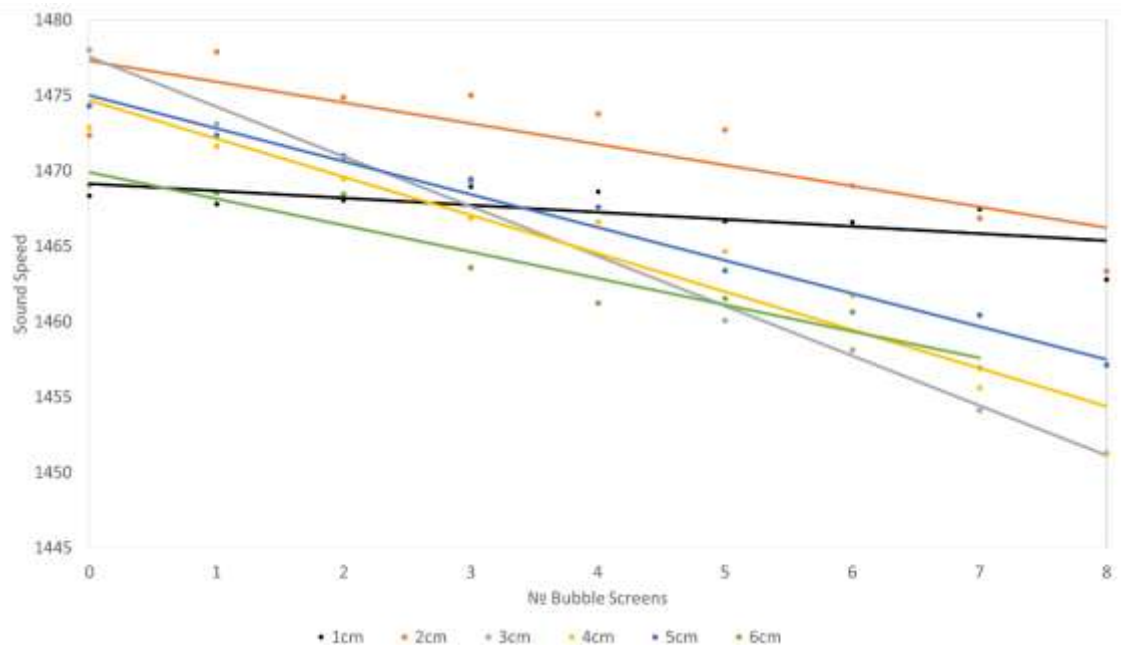

Figure 5.1: Phase speed as a function of the number of bubble screens in the system for each screen separation from 1 cm to 6 cm.

The uncertainty in the initial frequency calculation used for the duration of this experiemnt would produce a systematic error in sound speed measurements of 15ms^{-1}. The proportional change remains unaffected as the same frequency value

was used throughout. The random error in each sound phase speed calculation is therefore dependent upon the uncertainty in the measurement of the wavelength used in equation 3. This uncertainty was ± 0.02 mm on the vernier calipers for a measurement of 20λ, giving a ± 0.001 mm uncertainty in λ. This results in a phase speed uncertainty of ± 0.2 ms^{-1}.

The trends in each case follow a linear regression showing a constant decrease in sound speed per bubble screen added, as might be expected. This linear nature of regression contrasts the results obtained in the previous study by Fairman, which found a non linear, increasing rate of decay at close separations (Fairman, 2014). Fairman's study suffers from a limited data set. Without a more detailed methodology, it is difficult to comment on the suitability of his methods, and the implications on the differing results of the studies.

The rate of sound speed loss in each case is different. Table 1 displays the gradient of the linear trend for each screen separation, and its associated error. These were then plotted in figure 5.2.

Table 1: Sound speed decay rates calculated from the gradients of figure 5.1 and their associated errors.

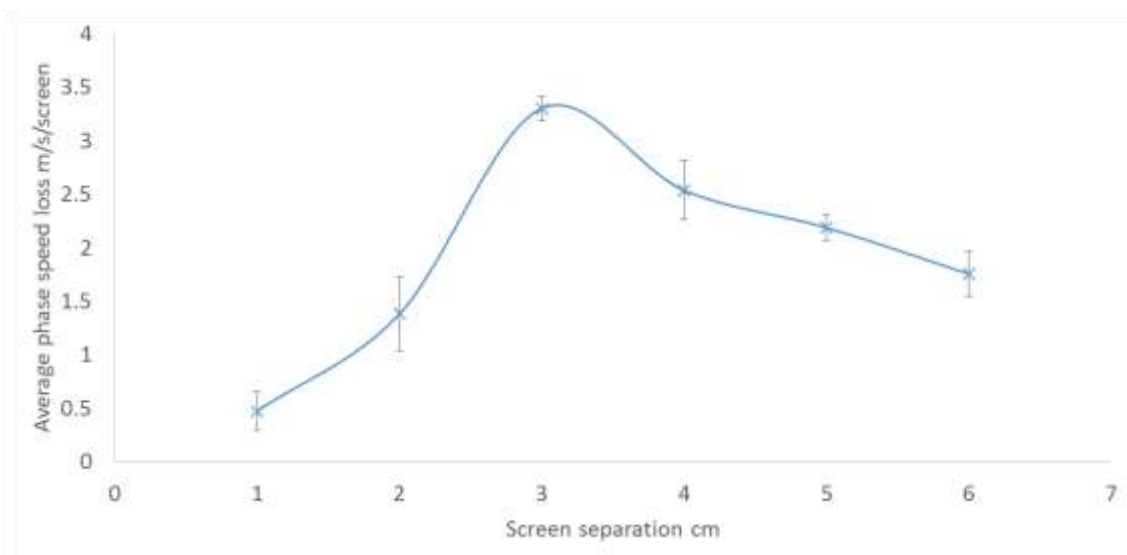| Separation	Gradient m/s/screen	Standard Error m/s/screen
1cm	-0.5	0.2
2cm	-1.4	0.3
3cm	-3.3	0.1
4cm	-2.5	0.3
5cm	-2.2	0.1
6cm	-1.8	0.2

Figure 5.2: Sound speed decay rates calculated from the gradients of figure 5.1 and their associated errors plotted against screen separation.

A peak rate of phase speed loss per screen added was found at a screen separation of 3cm. Two methods were used to test the significance of this peak rate of loss; firstly it was hypothesised that the decay increased linearly with screen separation.

A linear increase in decay with screen separation results in a linear regression gradient of 0.23. Regressional statistics are included in table 2.

Table 2: Regression statistics for a linear model of phase speed loss with screen separation.

Mean x	3.5
Gradient	0.23038
Intercept	1.133153
Standard Deviation	0.234269
Error Sum of Squares	3.841729
t-value	-2.77645
Sum Squared Error from x̄	17.5

From these statistics, the 95% confidence interval of any predicted intensity loss (y) rate at a given separation (x_p) can be calculated from the following equation (Morrison, 2014):

Prediction interval for the new value of y at x_p

$$\left(\hat{m}x_p + \hat{b}\right) \pm t_{\alpha/2, n-2} s_{y,x} \sqrt{1 + \frac{1}{n} + \frac{\left(x_p - \bar{x}\right)^2}{SS_{xx}}} \qquad (4)$$

Where m is the gradient, b is the intercept, $t_{\alpha/2, n-2}$ is the t-value for the sample, $s_{y,x}$ is the standard deviation of slope, n is the number of samples, and SS_{xx} is the sum of the square errors of the x values from their mean.

As a new y value at the chosen x value will be subject to random variations in the data, this equation was used as it accounts for the effect of random variability in the data values used for the initial linear regression in calculating the confidence interval (Montgomery and Runger, 2011). This results in a maximum and minimum rate of loss at 3cm separation of 2.59 ms⁻¹screen⁻¹ and 1.06 ms⁻¹screen⁻¹ respectively. Figure 5.3 shows these limits superimposed upon the graph.

The value of the peak rate of loss at 3cm of 3.3 > 2.59 ms⁻¹screen⁻¹, and the lower limit of its error bounds lies above the upper maximum explainable decay as seen in figure 5.3, therefore it is unexplained by random variations in a linear model.

The second possibility was the peak was due to random error about a mean rate of intensity loss per added screen, assuming no trend with separation. This was tested by calculating the upper and lower limits of two standard deviations from the mean. These were 2.92 ms⁻¹screen⁻¹ and 0.96 ms⁻¹screen⁻¹ respectively. Therefore the peak rate of loss was not explained by this factor either.
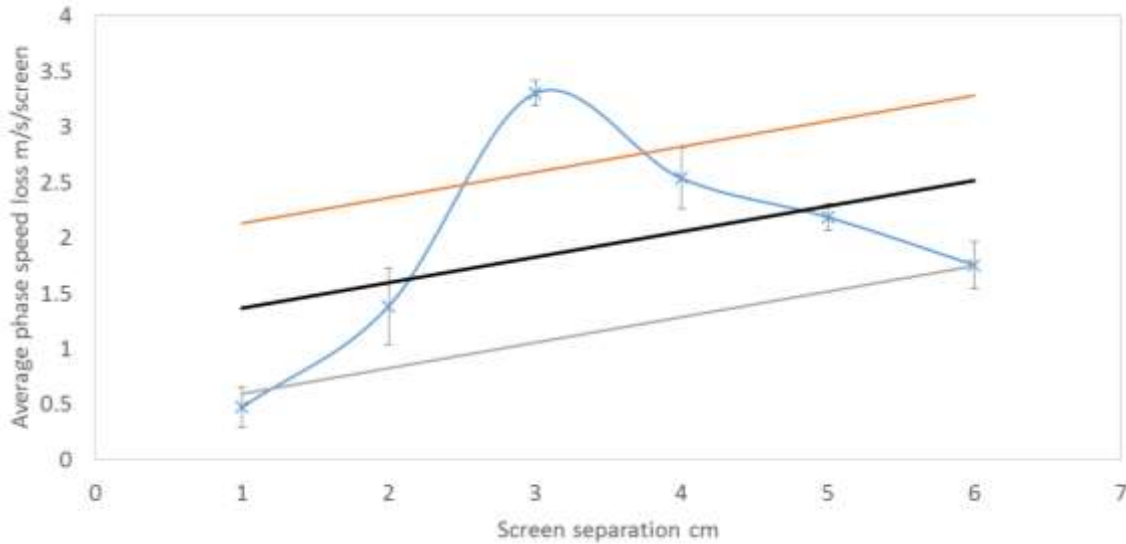
Figure 5.3: Sound speed decay rates calculated from the gradients of figure 5.1 and their associated errors plotted against screen separation. Superimposed are the linear trend and its associated 95% confidence limits.

To further investigate this peak it was important to adjust for the effects of void fraction on sound speed in the water column. The void fraction of the water column was determined for 1 to 8 bubble screens using the following formula:

$$For\ n = number\ bubble\ screens$$
$$b = number\ of\ bubbles\ per\ 100cm^2$$
$$r = bubble\ radius$$
$$nb = number\ of\ bubbles\ in\ cloud$$
$$d = transducer - hydrophone\ separation \approx 0.8m$$
$$\alpha_w = void\ fraction\ of\ the\ water\ column$$
$$Air\ volume = nb \times \frac{4}{3}\pi r^3$$

$$\alpha_w = \frac{Air\ Volume}{Total\ Volume} = \frac{nb \times \frac{4}{3}\pi r^3}{d \times 0.1^2} \qquad (5)$$

The results are shown in table 3.

Table 3: Calculated void fraction of the water column for 1 to 8 bubble screens.

Number of Screens	Void Fraction %
1	0.032
2	0.064
3	0.095
4	0.127
5	0.159
6	0.191
7	0.223
8	0.254

To allow comparability in the data it was also important to account for different reference bubble free sound speeds determined at the start of each round of data collection. Therefore the phase speed change from the reference speed is more suitable as a measure of the effect upon sound speed. In figure 5.4, phase speed change from the reference bubble free speed is plotted as a function of bubble screen separation for lines of constant void fraction corresponding to a constant number of screens in the system at different separations, as calculated in equation 5 (table 3).

Non-uniformity of the bubble sizes resulted in an associated error in the calculated void fractions. The bubble sizes ranged from 1mm to 5mm in diameter, with a mean diameter of 3.0 ± 0.4mm resulting in a proportional error in the calculated bubble volumes of 0.4 × volume. This resulted in a final void fraction error of ± 40%. To reduce this error a method of creating a more uniform bubble size distribution would be required.
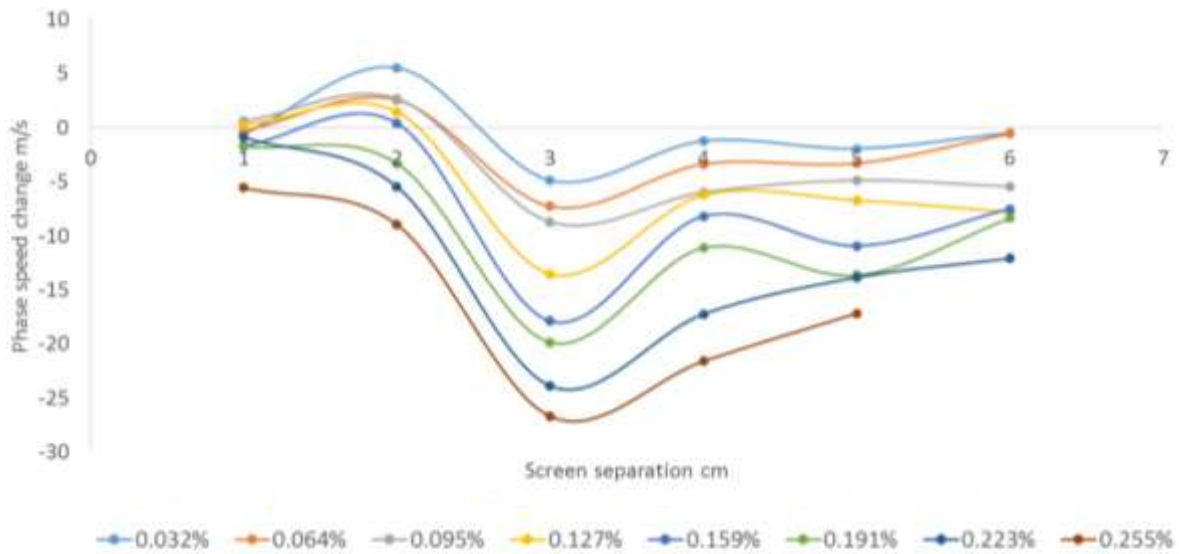

Figure 5.4: Phase speed change from the reference speed as a function of the screen separation for void fraction proportional to the number of screens in the system.

The 0.032% void fraction line shows some variation in phase speed change. This line corresponds to a single bubble screen in the system in each case, and as such it would be expected that the phase speed change should be even throughout. An attempt to adjust for this discrepancy was made. A mean phase speed change for 1 bubble screen was calculated as -0.604ms^{-1}. The variation of the 0.032% line from the mean was calculated for each separation experiment. The results are shown in table 4.

Table 4: Variation of the measured phase speed change from reference (for 0.032% void fraction) from a calculated average phase speed change.

Screen Separation	Variation from $\bar{x}$
1	0.018
2	6.131
3	-4.279
4	-0.636
5	-1.349
6	0.116

This variation was applied to each void fraction to adjust the data. Figure 5.5 shows the adjusted results. A peak loss in phase speed remains present at 3cm separation.
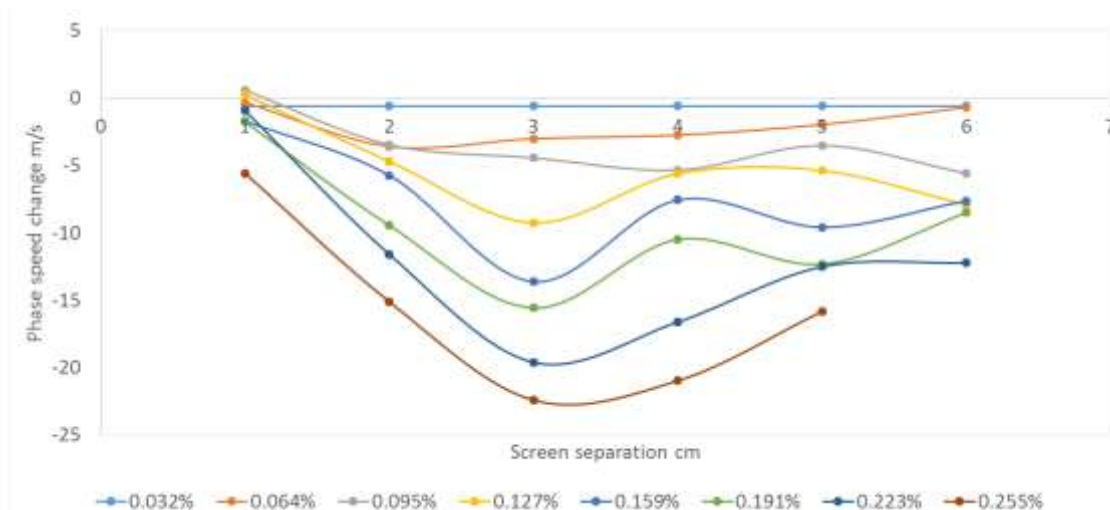

Figure 5.5: Adjusted phase speed change from the reference speed as a function of the screen separation for void fraction proportional to the number of screens in the system. See table 4 for adjustment values.

This peak phase speed change is unexplained by the effects of bubble proximity which would suggest a greater phase speed loss at 1cm separation (Nikolovska, 2007). It remains present when void fraction effects are adjusted for and random variations between experiments are filtered out. The low effect upon sound speed attributable to void fraction, corresponding to the separation between lines in figure 5.5, may be expected, as at high frequencies relative to the resonant bubble frequency sound speed is asymptotic towards the reference bubble free speed (figure 3.1; (Medwin, 1975; Urick, 1967)). The bubbles in this experiment had a radius of 1.5mm. From Equation 1, their corresponding Minnaert frequency was 1.996 kHz ~ 2 kHz. Therefore the transmitted frequency of 195 kHz was very large relative to the resonance of the bubbles. Equally the resonant frequency of the bubble layers is smaller than the resonant frequency of the component bubbles (Lu, 1990) and will be low compared to the operational frequencies of this experiment.

A further line of enquiry would be into the wavelength of the sound wave and its interactions with the bubble layers. The effect on sound speed of the relative position of individual bubbles to each other has been investigated, finding that if the spacing between bubbles is significantly closer than the wavelength of the incident sound wave, there will be an effect upon the speed of sound (Wildt, 1968). The spacing of bubble screens and their relation to incident wavelength remains an area for study. At 195 kHz the wavelength approximated 7.5mm. A 3cm screen separation corresponds closely to a distance of four wavelengths. In order to investigate the impact of wavelength upon sound speed loss, further experiments at frequencies corresponding to screen separations of 1 to 6cm are justified. The intent was to investigate these in the course of this project, however limitations of the transducer resonant frequencies meant frequencies below 97.5 kHz were unable to be investigated. This was due to the piston transducers inherent properties meaning it could only transmit at integer multiples of its resonant frequency, or at half its resonant frequency. Frequencies useful for further investigation are shown in table 5.

This is an area of potential for future research and would require different transducers to implement.

Table 5: Frequencies and their approximate wavelengths for a sound velocity of 1480 ms^{-1}.

Approximate wavelength cm	Frequency kHz
1	148.0
2	74.0
3	49.3
4	37.0
5	29.6
6	24.7

A further analysis of the phase speed change within the bounds of the bubble system was conducted. If the region between the first and last bubble screen in the system is taken to be a region of uniform density equal to the composite of the density of the water and the volume of air within it, essentially assuming a homogeneous fluid of averaged density, the sound speed change within the bounds of the bubble screens can be calculated assuming a constant bubble free speed throughout the unbounded water column (Figure 5.6).
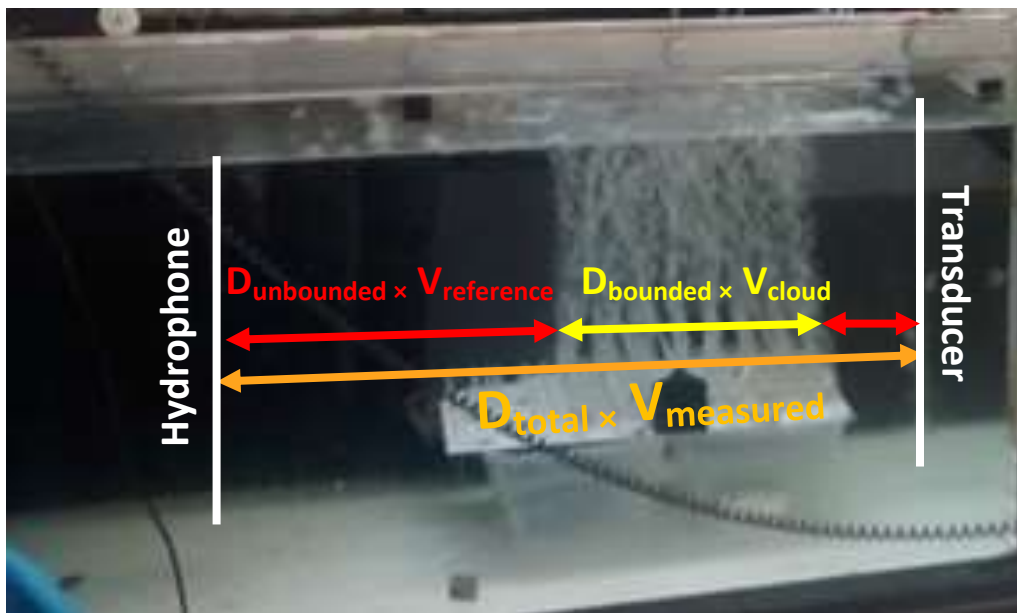

Figure 5.6: Visualisation of bubble system boundaries used for calculation of phase speed change within the bounds of the bubble cloud.

For a total distance D_{total} = 0.8m, the adjusted speed V_{cloud} for *n* screens at *s* separation was calculated as follows:

$$D_{total}V_{measured} = D_{unbounded}V_{reference} + D_{bounded}V_{cloud}$$

$$D_{unbounded} = D_{total} - D_{bounded}$$

$$D_{bounded} = 0.01ns \; for \; n > 1 \; or \; 0.01n \; for \; n \leq 1$$

$$\therefore V_{cloud} = \frac{0.8 V_{measured} - (0.8 - 0.01ns)V_{reference}}{0.01ns}$$

$$V_{cloud} = \frac{0.8(V_{measured} - V_{reference}) - 0.01ns V_{reference}}{0.01ns}$$

$$V_{cloud} = \frac{0.8}{0.01ns}(V_{measured} - V_{reference}) - V_{reference} \tag{6}$$

This adjusted speed is presented in figure 5.7. The magnitudes of the changes in sound speed are considerably greater within the confines of the bubble cloud. As this is assuming a homogeneous region of composite density with a uniform sound speed in the region bounded by the bubble screens, the actual sound speed variations within the screens are likely to be even greater.

Figure 5.7 shows lines of constant void fraction within the water column as a whole between the transducer and hydrophone. When considering the speed variations within the cloud, constant void fractions correspond to constant bubble screen separations and the void fraction is independent of the number of bubble screens in the system. Figure 5.8 shows the sound speed change within the cloud as a function of the number of bubble screens added to the system (independent variable) for lines of constant cloud void fraction (dependent upon screen separation). From this figure, phase speed change within the cloud appears independent of the number of screens within the cloud at the majority of separations. The primary factor affecting phase speed change within the cloud is the screen separation, with a maximum phase speed loss at 3cm separation as discussed previously.
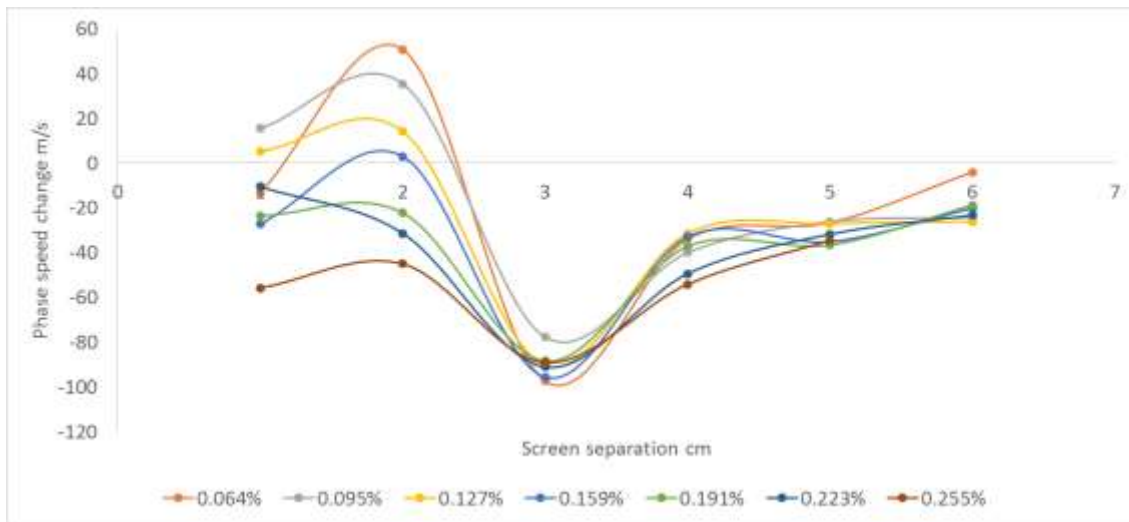

Figure 5.7: Adjusted phase speed change within the bounds of the bubble screen system for water column void fractions proportional to the number of screens in the system.
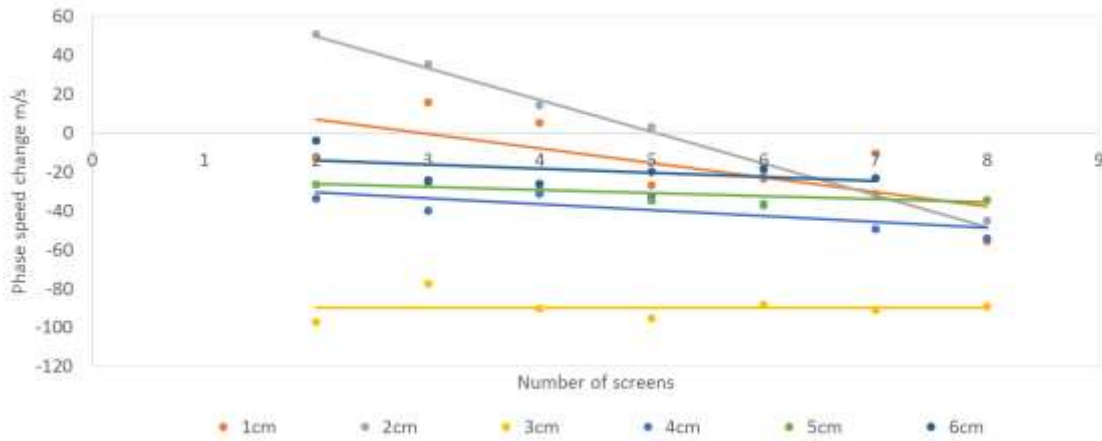
Figure 5.8: Adjusted phase speed change within the bounds of the bubble screen system as a function of the number of screens in the system for screen separations of 1 cm to 6cm.

Sound speed variations at 500 kHz were indistinguishable beyond the random fluctuations due to temperature variations during the course of the experiment, and the results have not been included in the body of this report. See appendices for reference.

The next phase was to investigate the effect of void fraction within uniform bubble clouds upon phase speed.

5.1.2. Clouds

Bubble size distributions were found to be insignificantly affected by variations in air output within the operational range. The output bubble count of each line was tested, and an average taken of all eight for every air output level. This was used alongside the average bubble diameter of 3.0mm ± 0.4mm to calculate the void fraction of the bubble cloud at each output level. An example calculation is below for a 10cm × 10cm cloud cross-section:

$$For\ n = number\ bubble\ screens$$
$$b = number\ of\ bubbles\ per\ 100cm^2$$
$$r = bubble\ radius$$
$$nb = number\ of\ bubbles\ in\ cloud$$
$$Air\ volume = nb \times \frac{4}{3}\pi r^3$$
$$Total\ cloud\ volume = 0.01n \times 0.1^2$$

$$\therefore Void\ Fraction, \alpha = \frac{nb \times \frac{4}{3}\pi r^3}{0.01n \times 0.1^2} \tag{7}$$

$$\alpha = \frac{4b\pi r^3}{0.03 \times 0.1^2}$$

$$For\ r = 0.0015 \Rightarrow \alpha = 4\pi b \times \frac{0.0015^3}{0.0003}$$

$$\alpha = 4.5 \times 10^{-5}\pi b \tag{8}$$

For a transducer-hydrophone separation of 0.5m (separation during the cloud experiment) the void fraction of the water column from equation 5:

$$d = 0.5m$$

$$\alpha_w = \frac{nb \times \frac{4}{3}\pi r^3}{0.5 \times 0.1^2}$$

$$\alpha_w = 9 \times 10^{-7}\pi nb$$

$$\alpha_w = 7.2 \times 10^{-6}\pi b \quad for\ n = 8$$

The results of the above calculations are shown in table 6. There is an associated void fraction uncertainty of ±40% as discussed previously.

Table 6: Bubble cloud and water column void fraction measurements for the air pump output levels used in this experiment.

Air Output Level	Bubbles/ 100cm^2	Cloud Void Fraction %	Water Column Void Fraction %
0	0	0.00	0.00
1	106	1.50	0.24
2	121	1.71	0.27
3	125	1.77	0.28
4	136	1.92	0.31
5	141	1.99	0.32
6	148	2.09	0.33
7	149	2.11	0.34
8	158	2.23	0.36
9	149	2.11	0.34
10	170	2.40	0.38
11	180	2.54	0.41

Phase speed data was plotted against void fraction (Figure 5.9). Phase speed appears to show the beginning of an inverse square or exponential decay relationship with increasing void fractions. This corresponds to results obtained in the sea surface bubble layers in experiments by Farmer and Vagle using an upward looking sonar examining the phase speed loss in the sea surface bubble layer, and discussed in a paper by Buckingham (Farmer, 1989; Buckingham, 1997). Their results are shown in figure 5.10 for comparison. Their data is presented as a depth profile; bubble concentration decreasing with depth.

This experiment was limited by the minimum output level of the air pump and the minimum bubble size such that at its lowest bubble output, void fraction remains relatively high compared to natural observations at 0.25%, and due to the bubble diameter of 3.0mm, much of this concentration of air is contained in relatively few bubbles, meaning this experiment is limited in its ability to approximate homogeneous models of bubble cloud acoustics. The next phase of the discussion looks at the effects of bubble clouds and screens on attenuation.

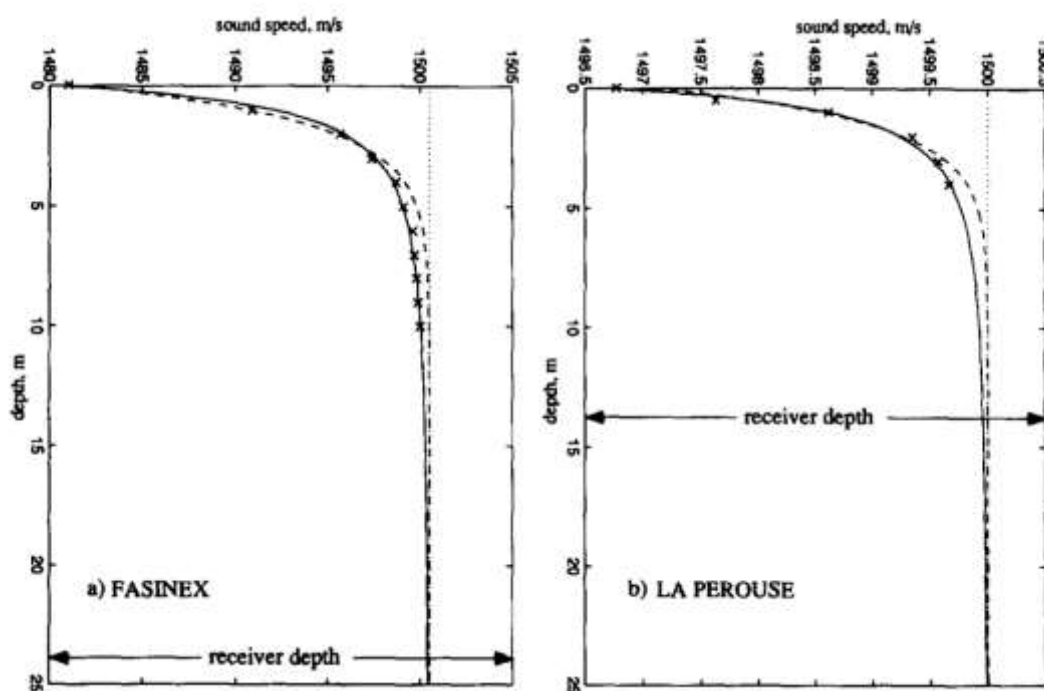**Figure 5.9:** Phase speed profile with reducing void fraction for 195 kHz.

Figure 5.10: Phase speed profile with depth for measurements taken at two locations, Fasinex and La Perouse (Farmer, 1989; Buckingham, 1997). Void fraction due to wave breaking reduces with depth.

5.2. Attenuation

5.2.1. Screens

Target intensity averages were plotted against the number of bubble screens in the system for each screen separation from 1 to 6 centimetres. From figure 5.11 it is apparent the target intensity decreases exponentially with additional screens in the system. This is expected, as the target intensity decreases by a certain proportion per screen of bubbles in the system. The results were plotted on a natural logarithmic scale (figure 5.12) with the number of screens converted to their respective void fractions, and the gradients determined through linear regression. These results are shown in table 7. The gradient represents the power of the exponent term and hence the decay rate. The magnitude of the decay rates were plotted in figure 5.13 against screen separation.
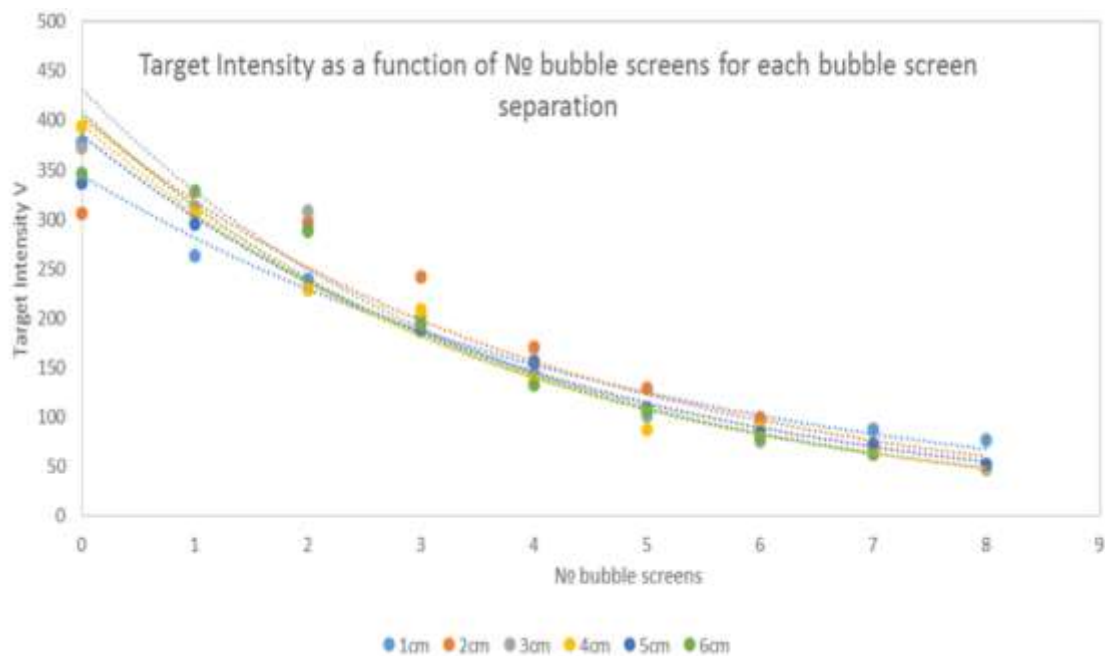

Figure 5.11: Target intensity as a function of the number of bubble screens in the system at 500 kHz for screen separations 1 cm to 6 cm.
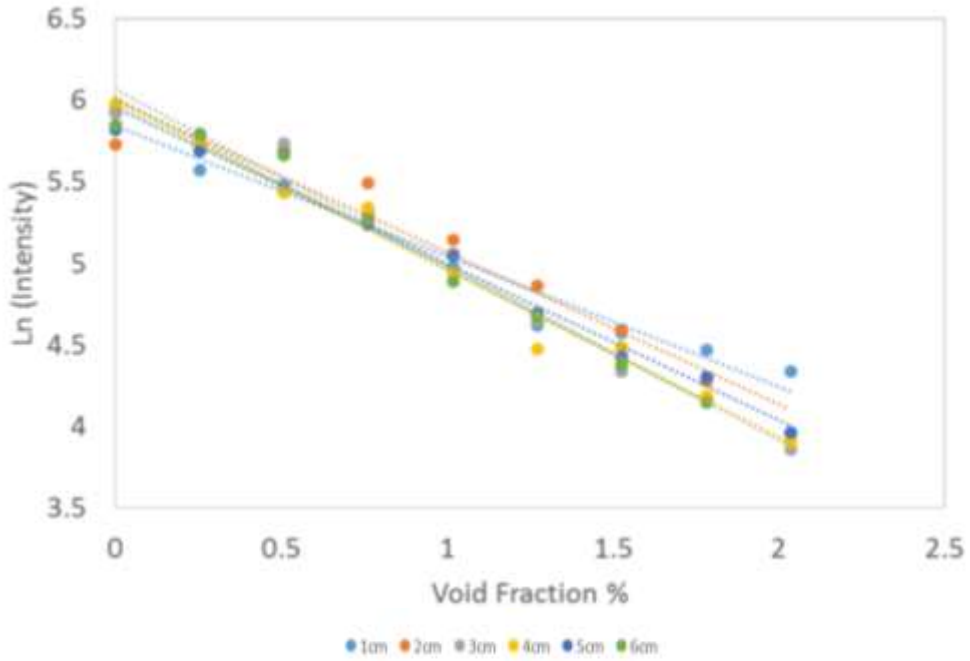
Figure 5.12: Natural logarithm of target intensity as a function of the number of bubble screens in the system at 500 kHz for screen separations of 1 cm to 6 cm. The x scale is presented as the equivalent void fraction proportional to the number of screens.

Table 7: Gradients and uncertainties determined from regressional analysis of target intensity decay with void fraction. Gradients are equivalent to the exponential decay factor for each screen separation at 500 kHz.

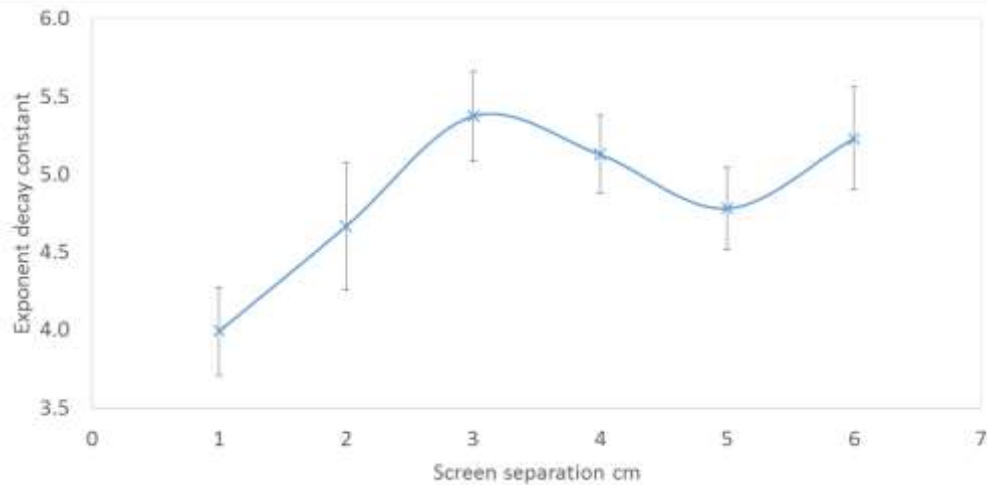| Separation	Gradient	Standard Error
1cm	4.0	0.3
2cm	4.7	0.4
3cm	5.4	0.3
4cm	5.1	0.2
5cm	4.8	0.3
6cm	5.2	0.3

Figure 5.13: Exponential decay factor for each screen separation at 500 kHz, and its associated uncertainty.

[135]

A peak decay was seen at 3cm separation, rising again at 6cm separation. Two methods were used to test the significance of this peak decay as in section 5.1.1; firstly it was hypothesised that the decay increased linearly with screen separation.

A linear increase in decay with screen separation results in a linear regression gradient of 0.179686. Regressional statistics are included in table 8. From these the statistics the 95% confidence interval of any predicted intensity loss (y) rate at a given separation (x_p) was calculated from equation 4 (Morrison, 2014):

Table 8: Regression statistics for a linear model of decay rate increase with screen

Mean x	3.5
Gradient	0.179686
Intercept	4.231267
Standard Deviation	0.100298
Error Sum of Squares	0.704177
t-value	-2.77645
Sum Squared Error from X̄	17.5

separation at 500 kHz.

This results in a maximum and minimum rate of decay at 3cm separation of 5.07V/screen and 4.47V/screen respectively. Figure 5.14 shows these limits superimposed upon figure 5.13. The value of the peak decay at 3cm of 5.4 > 5.07, and the lower limit of its error bounds lies above the upper maximum explainable decay as seen in figure 5.14, therefore it is unexplained by random variations in a linear model.
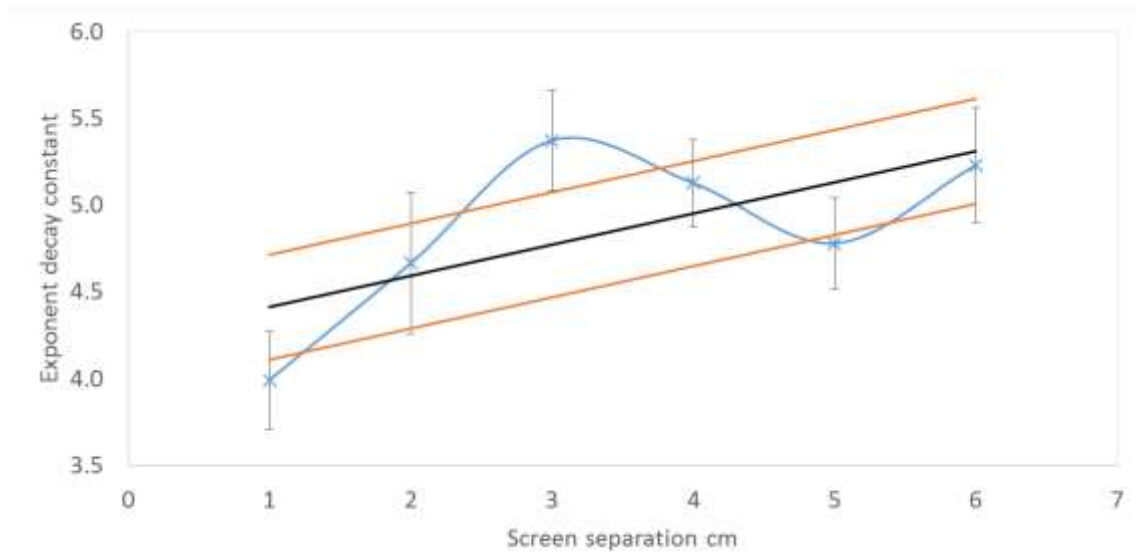

Figure 5.14: Exponential decay factor for each screen separation at 500 kHz, and its associated uncertainty as seen in figure 4.13. A hypothesised linear trend and its 95% confidence limits are superimposed.

The second possibility was the peak was due to random error about a mean rate of intensity loss per added screen, assuming no trend with separation as tested in

section 5.1.1. The upper and lower limits were 5.32V/screen and 4.4V/screen respectively, therefore the peak rate of loss was not explained by this factor either.

The data was converted to decibel form using the following equation:

$$\alpha = -20 \log_{10}\left({}^{V_n}\!/_{V_0}\right) \tag{9}$$

α = attenuation in decibels, V_n = Intensity for n screens, V_0 = Reference intensity.

This was analysed in the same manner as the intensity data, yielding the same significant peak attenuation rate at 3cm separations (figures 5.15 & 5.16).
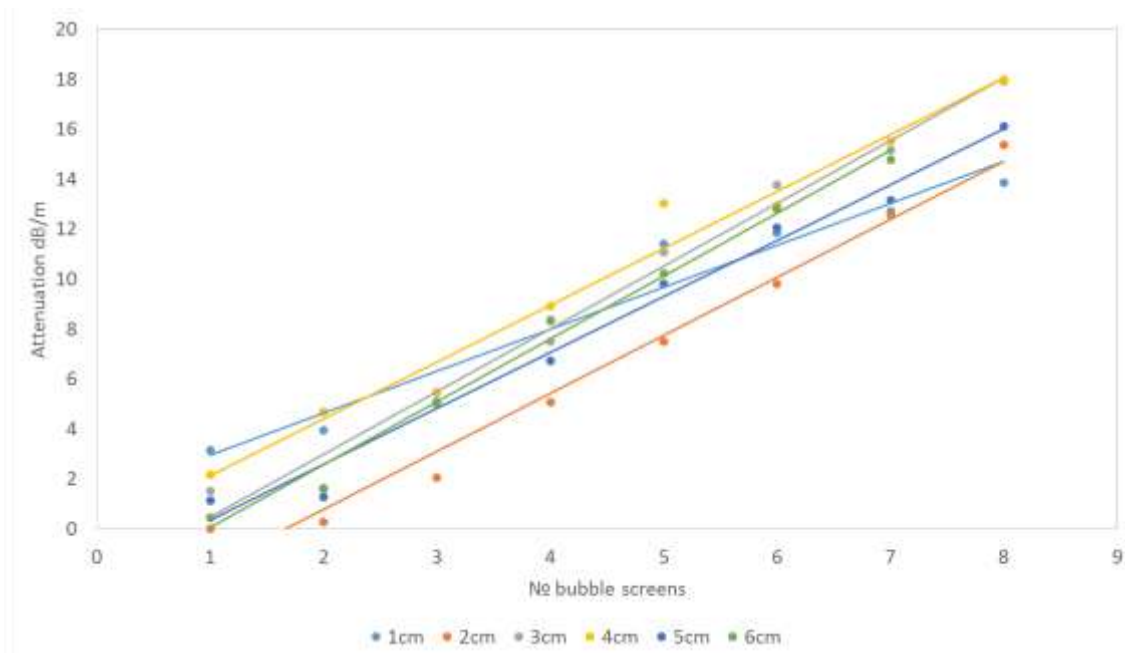

Figure 5.15: Attenuation as a function of the number of bubble screens in the system at 500 kHz for screen separations of 1 cm to 6 cm.
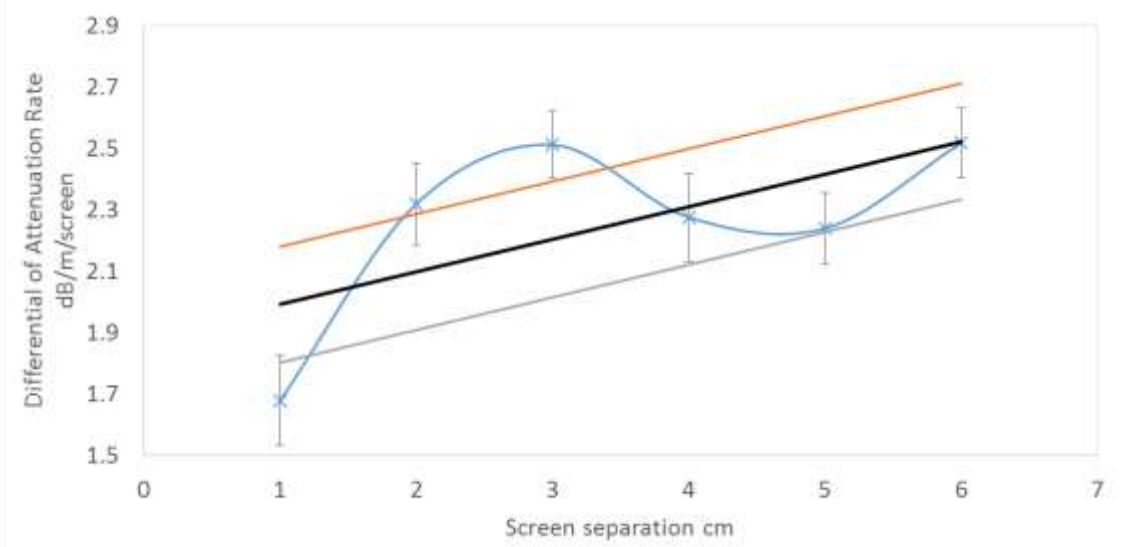

Figure 5.16: Attenuation rate per screen added against screen separation at 500 kHz. The hypothesised linear trend and 95% confidence limits are superimposed.

The lesser attenuation rates at close separations may be attributable to effects outlined by Nikolovska and Manasseh in a study on bubble chains which shows that acoustic energy can be channelled along chains of closely separated bubbles acting as coupled oscillators (Nikolovska, 2007). This study found attenuation could be up to 160dB/m less along the axis of the bubble chain. It is possible a similar effect occurs in this instance as the bubble screens become closer together. An investigation into the effect of wavelength on intensity loss is justifiable also in order to rule out wavelength interactions. Testing at frequencies outlined in table 4 may be beneficial to this investigation. As the wavelength at 500 kHz is approximately 3mm, this corresponds closely to the average bubble diameter in this experiment. An analysis of a greater range of bubble sizes may also prove beneficial.

For comparison with a sound wave of longer wavelength (~7.5mm), attenuation was recorded at 195 kHz for bubble screens and analysed as above. The results are shown in figure 5.17.
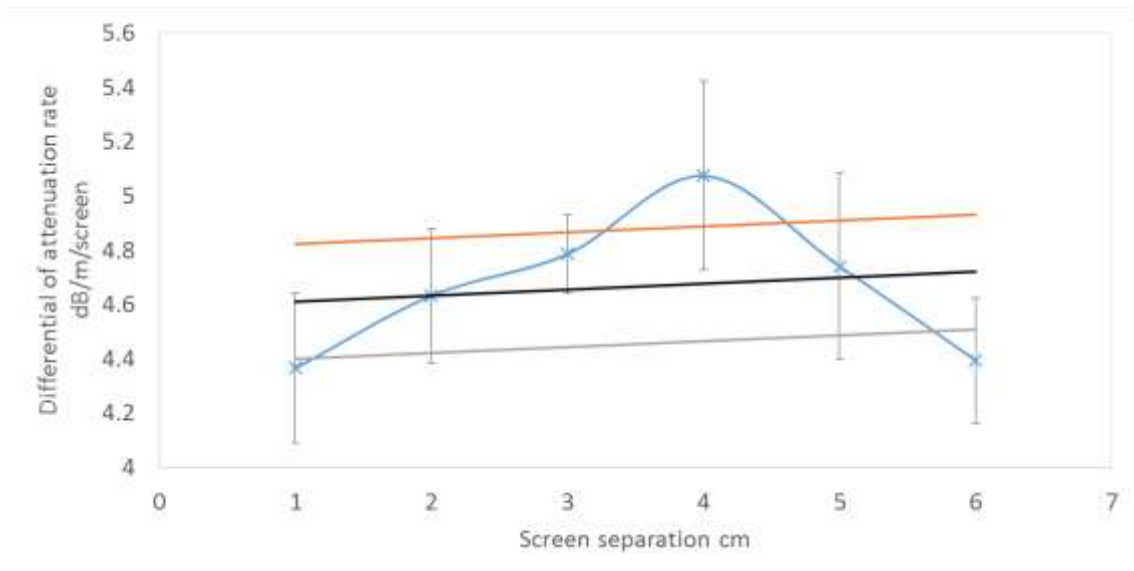

Figure 5.17: Attenuation rate per screen added against screen separation at 195 kHz. The hypothesised linear trend and 95% confidence limits are superimposed.

A peak was observed at 4cm screen separation. Hypothesising a linear trend results in the confidence limits superimposed on figure 5.17. There is no significant peak in this instance when the error bounds of the attenuation rate are considered. Assuming a random distribution about a mean attenuation rate resulted in upper and lower confidence limits of 5.15 dB/m/screen and 4.18 dB/m/screen respectively, therefore the peak at 4cm screen separation of 5.07 dB/m/screen is not significant in this case.

5.2.2. Clouds

Target intensity data for bubble clouds at varying void fractions outlined in table 5 were converted into decibel form using equation 9. This gave the attenuation for each void fraction (figure 5.18 below). At 500 kHz, attenuation appears to follow an exponential relationship with void fraction in this range approximated by the equation:

$$\alpha = \alpha_0 e^{2.17\beta}$$

Where α = attenuation and β = void fraction of the bubble cloud.

195 kHz appears to follow the relationship:
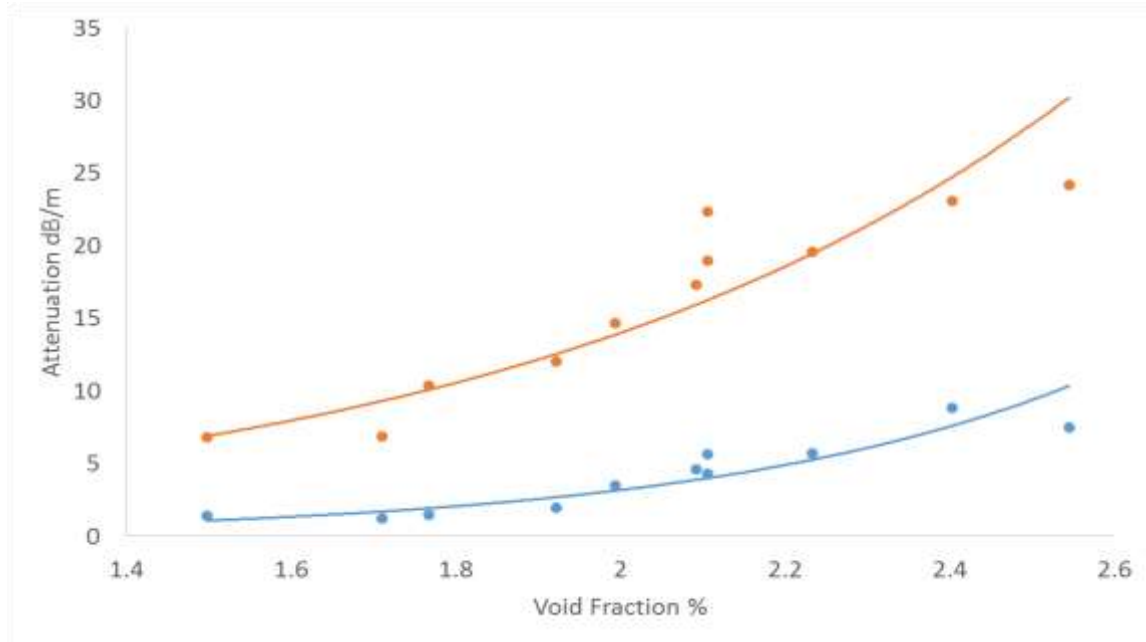
$$\alpha = \alpha_0 e^{1.41\beta}$$

Figure 5.18: Attenuation at 500 kHz (blue) and 195 kHz (orange) against void fraction within the bubble cloud.

To test the significance of these relationships in the data, regressional analysis was conducted on the attenuations natural logarithm against void fraction (figure 5.19).
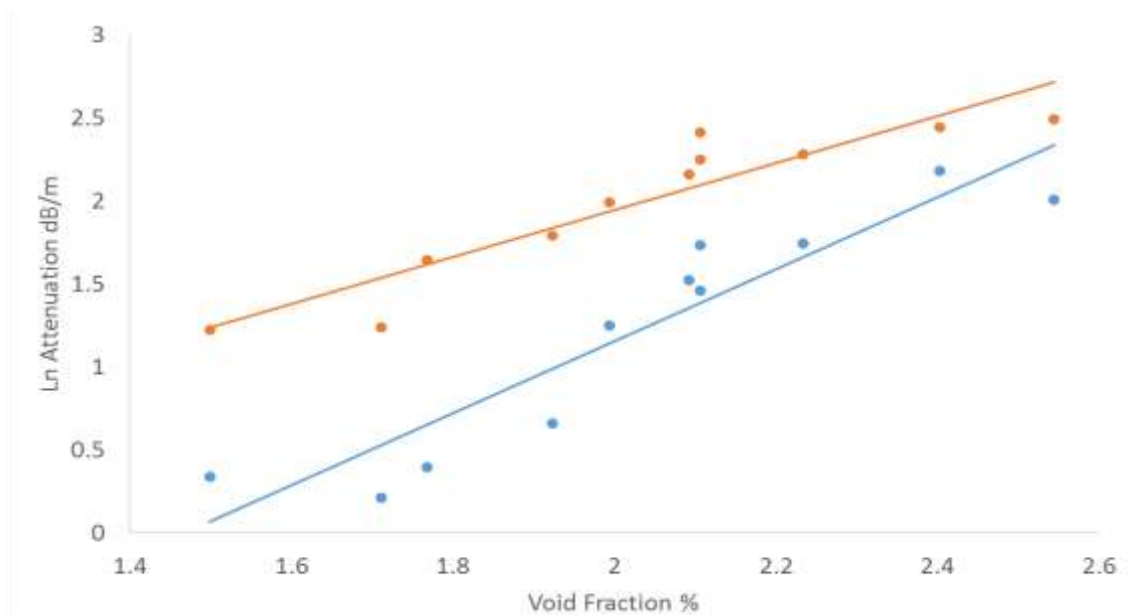

Figure 5.19: Natural logarithm of attenuation at 500 kHz (blue) and 195 kHz (orange) against void fraction within the bubble cloud.

This resulted in a P value of 2.68×10^{-5} for 500 kHz and 3.05×10^{-5} therefore it can be said the correlations are significant at the 95% confidence level and therefore the trends are a good fit for the data.

The 500 kHz data was measured as a target echo, and thus assumes no loss in intensity due to target strength in the calculations. The target was a large, smooth metal plate and as such should have a large target strength ratio. If this were factored into the calculations, a reduction in Target Strength results in a reduction in Transmission Loss for the same Echo Intensities recorded in this experiment (equation 10). Therefore the measured attenuation at 500 kHz is an overestimate.

Echo Intensity EL = Source Level SL – 2 Transmission Loss TL + Target Strength TS

$$\therefore TL = \frac{1}{2}(SL + TS - EL) \tag{10}$$

The 195 kHz data was recorded as a direct measurement of the acoustic signal by a hydrophone and as such is not subject to this consideration. Greater attenuation was seen at 195 kHz as opposed to 500 kHz. Attenuation has a frequency dependence governed in part by an inversion of an equation derived by Commander and Prosperetti (1989) and results in a peak attenuation at a frequency dependent upon the bubble cloud distribution and bubble properties with a decay at frequencies in excess of this peak (Weber, 2006). As the frequencies used in this experiment are large relative to the resonant frequency of the bubbles generated, they are likely to be situated along the tail of the attenuation distribution and this could explain the greater attenuation at the lower 195 kHz frequency.

5.3. Limitations

This study was subject to several limitations. Variability in the bubble sizes generated resulted in a large uncertainty in the void fraction estimations used in this study on the order of ±40%. The large bubble size additionally means that assumptions of homogeneity in the bubble cloud are unlikely to be a good approximation.

Furthermore, the frequency range applied in this study was limited by the resonant frequency of the transducers used such that frequencies below 195 kHz could not be tested. 20 kHz to 148 kHz covers the frequency range necessary to approximate wavelengths equivalent to the screen separations implemented in this study. This is an area for further study, requiring a different transducer to implement.

A further limitation was the temperature variability in the tank, on the order of one to two degrees Celsius per day, which had an effect upon the data such that temperature dependent phase speed fluctuations masked the results of the experiment at 500 kHz. A temperature controlled tank would be beneficial to control this variable.

Additionally, the range of void fractions produced by this methodology was limited to the output levels of the air pump. At low output levels, the bubble size was such that the air volume was concentrated in a small number of bubbles, and measurements may have approximated closer the reference value of the variable, and homogeneity is a poor approximation.

6.   Conclusions

Sound speed measurements were recorded and compared at 500 kHz and 195 kHz frequencies for bubble screens configured at different screen separations and bubble clouds of varying void fractions. At 195 kHz a significant peak rate of sound phase speed loss with added screens to the system was observed at 3cm screen separation, at the 95% confidence level. This peak remained present after effects of void fraction and cloud dimensions were moderated for in the data. This peak is unexplained by theoretical sound speed-frequency models for individual bubbles (Medwin, 1975; Urick, 1967), and bubble screens (Lu, 1990), or by bubble distribution models (Nikolovska, 2007) and may have a relation with wavelength as 3cm corresponded to four integer wavelengths. Further investigation at a range of wavelengths corresponding to screen separations is warranted and frequency suggestions are made in table 5. At the same 195 kHz frequency, bubble cloud phase speed measurements matched measurements made by upward looking SONAR systems in the natural environment (Farmer, 1989; Buckingham, 1997). At 500 kHz the phase speed change due to the bubbles in both the screen and cloud configurations was indistinguishable beyond phase speed fluctuations attributed to temperature fluctuations in the tank over the course of the experiment. This suggested the phase speed changes were small relative to the changes at 195 kHz, which may be attributable to 195 kHz closer proximity to the resonant frequency of the bubbles used in this experiment.

Attenuation measurements were also recorded and compared for 500 kHz and 195 kHz frequencies for screen configurations at different screen separations and cloud void fractions. For bubble screens, a peak decay was again observed at 3cm screen separations for 500 kHz frequency and was deemed significant at the 95% confidence level, however at 195 kHz there was no peak at 3cm, and the peak observed at 4cm screen separation was deemed not to be significant once errors were taken into consideration. Low attenuation rates were observed at close screen separations at 500 kHz and could be explained by bubbles acting as coupled oscillators (Nikolovska, 2007). Testing at the frequencies outlined in table 5 may be beneficial to further investigation.

Bubble cloud attenuation was observed to closely fit an exponential rise in attenuation with increasing void fraction, at the 95% confidence level. Greater levels of attenuation were observed at 195 kHz compared to 500 kHz which could be explained by frequency dependence of attenuation such that attenuation decays as frequencies increase beyond a peak attenuative frequency governed by statistical distributions of bubbles within the cloud and bubble radius (Commander & Prosperetti, 1989; Weber, 2006).

This study aimed to investigate the effects of bubble screen separation and bubble cloud void fraction on (1) phase speed and (2) attenuation of sound waves at frequencies comparable to frequencies used in commercial sonar applications. Two frequencies were tested at 195 kHz and 500 kHz which correspond to frequencies used in multibeam bathymetric sonar operations and high frequency side scan sonar imaging. For the aim (1), building on previous work testing the effects of bubble screens on sound speed (Fairman, 2014), a greater range of screen separations were tested. In contrast to the results of the previous study, a peak phase speed loss was found at 3cm screen separation, observing a linear trend throughout. To satisfy

aim (2) of the investigation, to measure the effect of screen separation and bubble cloud void fraction on attenuation, attenuation was measured for both frequencies at a range of 11 quantified cloud void fractions and compared, finding results that matched expected trends from theoretical studies. For screens, a peak attenuation was also observed at 3cm screen separation at 500 kHz, however no significant peak was found for 195 kHz. This investigation resulted in grounds for further investigations into the significance of sound wavelength on the change in phase speed and attenuation observed.

7.   Appendices
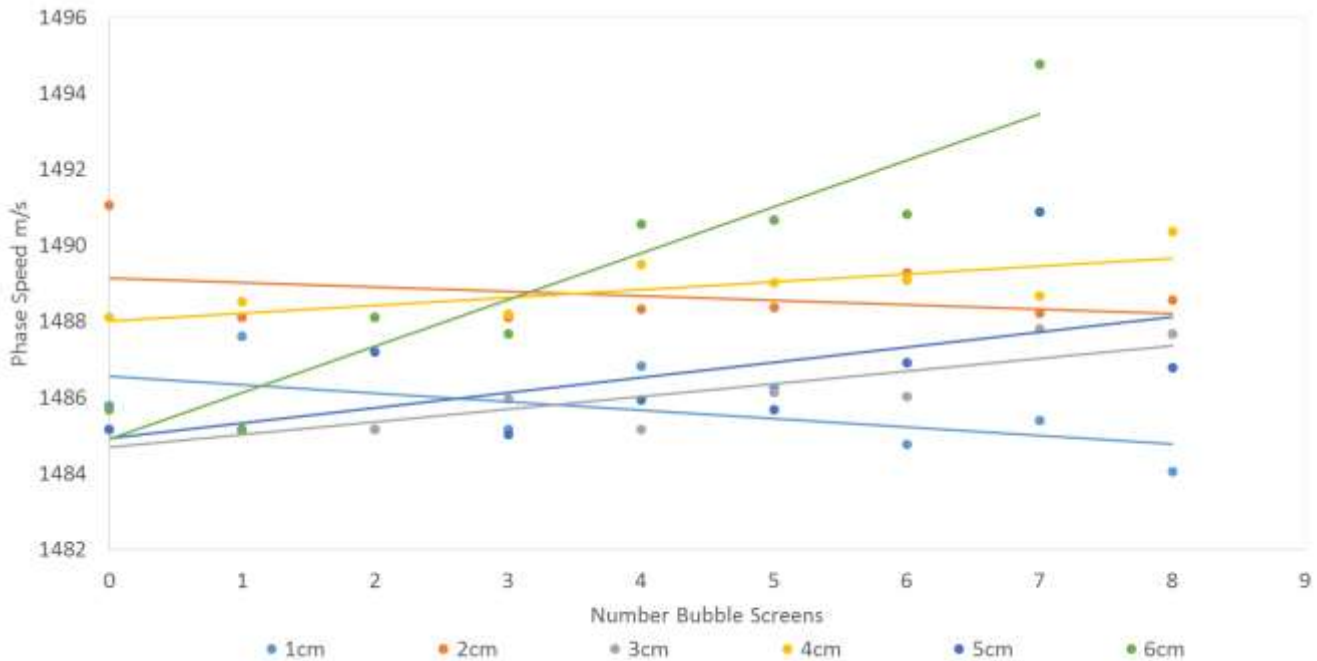
Appendix A: Sound speed at 500 kHz as a function of number of screens in the system for screen separations of 1 cm to 6 cm. Variability is within the range attributable to temperature fluctuations in the tank.

8.   References

Boyles, C.A., Rosenberg, A.P., & Qinqing, Z. (2013) Modelling the effect of bubble plumes on high frequency acoustic propagation in shallow water. *Oceans - San Diego.* 1 (8). p23-27.

Brekhovskikh L. M. & Lysanov Yu. P. (2001) *Fundamentals of Ocean Acoustics.* 3rd ed. Moscow: Springer. p25.

Buckingham, M. J. (1997) Sound Speed and Void Fraction Profiles in the Sea Surface Bubble Layer. *Applied Acoustics.* 51 (3). pW-250.

Chen, C.T. & Millero, F.J. (1977) Speed of sound in seawater at high pressures. *J. Acoust. Soc. Am.* 62 (5). p1129-1135.

Commander, K. W. & Prosperetti, A. (1989) Linear pressure waves in bubbly liquids: Comparison between theory and experiments. *J. Acoust. Soc. Am.* 19. 732-746.

Coppens, A. B. (1981) Simple equations for the speed of sound in Neptunian waters. *J. Acoust. Soc. Am.* 69 (3). p862-863.

Crawford G. B. & Farmer D. M. (1987) On The Spatial Distribution of Ocean Bubbles. *Journal of Geophysical Research.* 92 (C8). p8231-8243.

Del Grosso, V.A. (1974) New equation for the speed of sound in natural waters (with comparisons to other equations). *J. Acoust. Soc. Am* 56 (4). p1084-1091.

Doinikov, A.A., Manasseh, R., & Ooi. A. (2005) On time delays in coupled multibubble systems. *J. Acoust. Soc. Am.* 117 (1). p47–50.

Domenico, S. N. (1982) Acoustic wave propagation in air-bubble curtains in water; Part I, History and theory. *Geophysics.* 47 (3). p345-353.

Duro, V., Rajaona, D.R., Decultot, D., & Maze, G. (2011) Experimental Study of Sound Propagation Through Bubbly Water: Comparison with Optical Measurements. *IEEE Journal of Oceanic Engineering.* 36 (1). p114 & 125.

Fairman, M. (2014) The effect of oceanic bubbles on sound propagation underwater: how bubble plume size, spatial variation and density affect phase speed. *Plymouth University.*

Farmer et al. (2001) The Influence of Bubble Clouds on Acoustic Propagation in the Surf Zone. *Journal of Oceanic Engineering.* 26 (1).

Farmer, D. & Ming Li. (1994) Patterns of Bubble Clouds Organised by Langmuir Circulation. *Journal of Physical Oceanography.* 25. p1426-1440.

Farmer, D. M. & Vagle, S. (1989) Waveguide propagation of ambient sound in the ocean-surface bubble layer. *J. Acoust. Soc. Am.* 86. p1897-1908.

Giese, O. & Wise. Jr. J. E. (1994) *Shooting the War: The Memoir and Photographs of a U-Boat Officer in World War II.* Annapolis: Naval Institute Press. p145.

Hwang, P. A. & Teague, W. J. (2000) Low-Frequency Resonant Scattering of Bubble Clouds. *J. Atmos. Oceanic Technol.* 17. p847–853.

Lamarre, E. & Melville W. K. (1994) Sound speed measurements near the ocean surface. *J. Acoust. Soc. Am.* 96 (6), p3605-3616.

Leighton, T. G. (1994) *The Acoustic Bubble.* London: Academic Press Ltd.

Leighton, T.G., Walton, A.J. (1987) An experimental study of the sound emitted from gas bubbles in a liquid. *Eur. J. Phys.* 8. p98-104.

Lu et al. (1990) Underwater noise emissions from bubble clouds*. IEEE Journal of Oceanic Engineering.* 15 (4). p275-81.

Lurton, X. (2002) *An Introduction to Underwater Acoustics: Principles and Applications.* Chichester: Praxis Publishing Ltd.

Mackenzie, K.V. (1981) Nine-term equation for the sound speed in the oceans. *J. Acoust. Soc. Am.* 70 (3). p807-812.

Manasseh, R., Nikolovska, A., Ooi, A., & Yoshida, A. (2004) Anisotropy in the sound field generated by a bubble chain. *Journal of Sound and Vibration.* 278 (4–5). p807–823.

Medwin et al. (1975) Acoustic miniprobing for ocean microstructure and bubbles. *J. Geophys. Res.* 80. p405-413.

Medwin, H. & Clay, C. S. (1998) *Fundamentals of Acoustical Oceanography.* London: Academic Press Ltd. Chapter 8.

Minnaert, M. (1933) On musical air-bubbles and the sound of running water. *Philos. Mag.* 16. p235–248.

Montgomery, D. C. & Runger, G. C. (2011) *Applied Statistics and Probability for Engineers,* 5th edition, Wiley, New York. p422-423.

Morrison, F. A. (2014) Obtaining Uncertainty Measures on Slope and Intercept of a Least Squares Fit with Excel's LINEST. Available: *http://www.chem.mtu.edu/~fmorriso/cm3215/UncertaintySlopeInterceptOfLeastSquaresFit.pdf.* Last accessed 17th March 2015.

Nicholas et al. (1994) Sound emissions by a laboratory bubble cloud. *J. Acoust. Soc. Am.* 95. p3171.

Nikolovskaa A. & Manassehb, R. (2007) On the propagation of acoustic energy in the vicinity of a bubble chain. *Journal of Sound and Vibration.* 306 (3–5). p507–523.

Novarini, J.C., Keiffer, R.S. & Norton, G. V. (1998) A model for variations in the range and depth dependence of the sound speed and attenuation induced by bubble clouds under wind-driven sea surfaces. *IEEE Journal of Oceanic Engineering.* 23 (4). p423 & 438.

Sebastian, S.M. & Caruthers, J.W. (2001) Effects of Naturally Occurring Bubbles on Multibeam Sonar Operations. *MTS/IEEE Oceans.* 2. p1241.

Thorpe, S.A. (1982) On the Clouds of Bubbles Formed by Breaking Wind-Waves in Deep Water, and their Role in Air -- Sea Gas Transfer. *Philosophical Transactions of the Royal Society of London. Series A, Mathematical and Physical Sciences.* 304. P155-210.

Urick, R. J. (1967) *Principles of Underwater Sound.* 3rd ed. Los Altos, California: Peninsula Publishing. p249-254.

Weber, T. C. (2006) Acoustic propagation through bubble clouds. Doctor of Philosophy Thesis. The Graduate Programme in Acoustics. *Pennsylvania State University.*

Wildt, R. (1968) *Physics of sound in the sea. Part IV: Acoustic properties of wakes.* New York: Gordon and Breach. p29-30.

Wood, A. B. (1930) *A Textbook of Sound.* Third Ed. 1955. Bell. p360-362.

Würsig, B. et al. (2000) Development of an air bubble curtain to reduce underwater noise of percussive piling. *Marine Environmental Research.* 49. p79-93.

Yoon et al. (1991) An investigation into the collective oscillations of a bubble cloud. *J. Acoust. Soc. Am.* 89. p700.